Aus dem Pharmakologischen Institut

Direktor: Prof. Dr. Thomas Worzfeld

des Fachbereiches Medizin der Philipps-Universität Marburg

Transforming growth factor-β targets Formin-like 2 for Angiopoietin-like 4 secretion during the epithelial mesenchymal transition

Inaugural-Dissertation

zur Erlangung des Doktorgrades der Naturwissenschaften

(Dr. rer. nat.)

dem Fachbereich Medizin der Philipps-Universität Marburg

vorgelegt von

Christel Jessica Moussi

aus Bechmezzine El-Koura, der Libanon

Marburg, 2020

Angenommen vom Fachbereich Medizin der Philipps-Universität Marburg am:
31.03.2020

Gedruckt mit Genehmigung des Fachbereichs Medizin

Dekan: Herr Prof. Dr. H. Schäfer

Referent: Herr Prof. Dr. R. Grosse

1. Korreferent: Herr Prof. Dr. R. Jacob

Table of Contents

List of Figures

List of Tables

Abbreviations

2D	2-dimensional
3D	3-dimensional
ADP	Adenosine diphosphate
ANGPTL4	Angiopoietin-like 4
ANOVA	Analysis of variance
APS	Ammonium persulfate
Arp2/3	Actin-related proteins 2/3
ASB-14	Amidosulfobetaine-14,3-propanesulfonate
ATP	Adenosine triphosphate
BIM I	Bisindolylmaleimide I
BSA	Bovine serum albumin
°C	Celsius degree
DAD	Diaphanous autoregulatory domain
DAPI	4′, 6-Diamidin-2-phenylindol
DID	Diaphanous inhibitory domain
DMEM/F12	Dulbecco's modified eagle medium/ nutrient mixture F-12
DMSO	Dimethyl sulfoxide
DNA	Deoxyribonucleic acid
dNTP	Deoxynucleotide
ECM	Extracellular matrix
EDTA	Ethylenediamine tetraacetic acid
EMT	Epithelial to mesenchymal transition
FACS	Fluorescence-activated cell sorting
F-actin	Filamentous actin
FCS	Fetal calf serum
FMNL1	Formin-like 1
FMNL2	Formin-like 2
FMNL3	Formin-like 3
G-actin	Globular actin
GBD	GTPase binding domain
GFP	Green fluorescent protein
GST	Glutathione S-transferase
His	Histidine
Hr	hours
HRP	Horse-radish-peroxidase

IF	Immunofluorescence
IP	Immunoprecipitation
kD	Kilo Dalton
KO	Knockout
LPL	Lipoprotein lipase
µ	Micro
mA	milliampere
Min	minute
M	Molar
NP40	Nonidet P-40
NPF	nucleation promoting factor
PBS	Phosphate buffered saline
PBST	PBS/Triton-X
PCR	Polymerase chain reaction
PKC	Protein kinase C
qPCR	Quantitative polymerase chain reaction
RNA	Ribonucleic acid
Rpm	revolutions per minute
SDS	Sodium dodecyl sulfate
SDS-PAGE	Sodium dodecyl sulfate polyacrylamide gel electrophoresis
SEM	Standard error of the mean
siRNA	Small interfering ribonucleic acid
TBP	TATA-binding protein
TGF	Transforming growth factor
TPA	12-O-tetradecanoylphorbol-13-acetate
TriZol	Guanidium thiocyanate
WB	Western blot
WH2	WASP-Homology 2, Wiskott-Aldrich homology 2
WT	Wild type
Xg	G force

1. Introduction

1.1 The actin cytoskeleton

Cells, the basic unit of life, have the remarkable ability to change shape, divide, and move. These vital functions are powered by a dynamic assembly known as the cytoskeleton (Fletcher & Mullins, 2010). Eukaryotic cells contain three main types of cytoskeletal filaments: microfilaments, intermediate filaments, and microtubules. Actin filaments are the thinnest of the cytoskeletal filaments with a diameter of approximately 6-8 nm (Cooper, 2000). Various important cellular functions such as migration, invasion, endocytosis, adhesion, and cytokinesis require the rearrangement and remodeling of the actin cytoskeleton (Egea, Serra-Peinado, Salcedo-Sicilia, & Gutiérrez-Martínez, 2013; Nurnberg, Kitzing, & Grosse, 2011; Olson & Sahai, 2009; Parsons, Horwitz, & Schwartz, 2010; Pollard & Cooper, 2009).

Actin is a 42 kDa globular, highly conserved, and most abundant cytoskeletal protein in eukaryotic cells (Pollard, 2016). Actin exists in two different forms, globular and filamentous actin. G-actin is a globular monomer of 375 amino acids with a pointed and barbed end. G actin monomers polymerize to form actin filaments (Lee & Dominguez, 2010). Actin filament polymerization occurs over three phases: a nucleation phase, an elongation phase, and a steady state phase. During nucleation, three actin monomers usually form a trimer otherwise called ‘‘actin nucleus’’ (Sept & McCammon, 2001). In the elongation phase, monomers are rapidly added to the filament. Polymerization is reversible and proceeds from both ends to yield F-actin, a helical polymer. F-actin has structural polarity, a pointed (-) end and a barbed (+) end. The filament grows at both ends but growth is faster at the barbed (+) end (Pollard, 2016).

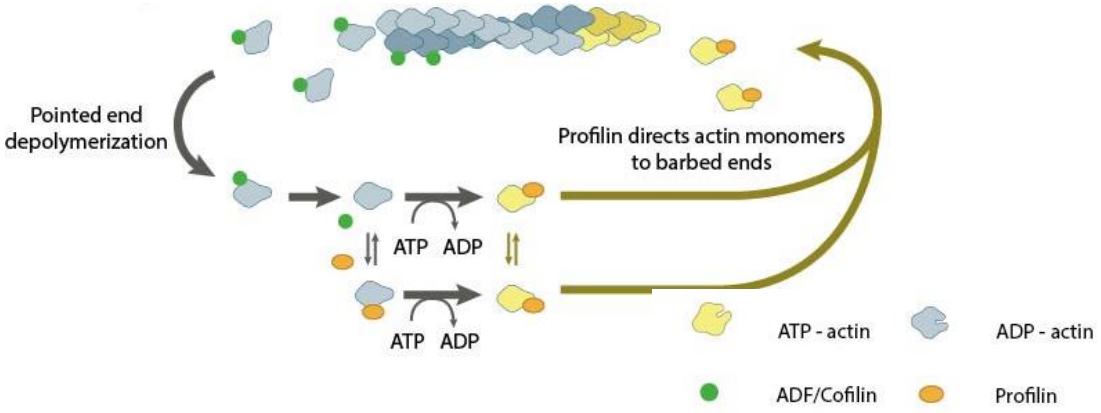

Figure 1. Actin filament treadmilling regulation.

Actin fibers are formed of 2 chains of polar actin subunits arranged in a double helix. Profilin forms a complex with ATP-actin, which directs actin monomers to the barbed ends. Upon ATP

exchange, ADP-actin dissociates from the pointed end. Factors such as ADF/Cofilin increase the rate of dissociation of ADP-actin at the pointed end. Adapted from MBInfo, 2018.

Actin filaments undergo treadmilling where there is a net gain of subunits on the barbed end and an equivalent net loss of subunits on the pointed end. ATP-binding on actin subunits modulates the dynamics of filament assembly, with ATP-binding generally favoring inter-subunit interactions and thereby filament assembly. At high free ATP-G-actin concentrations, the rate of addition exceeds the rate of dissociation and this results in actin filament growth. Soon after polymerization, ATP is hydrolyzed to ADP + Pi. ADP bound actin which is primarily at the pointed end of the filament, dissociates more readily than ATP bound actin (Fig.1). Hence, ATP binding and hydrolysis play a key role in the dynamic behavior of actin filaments (Bugyi & Carlier, 2010; Otterbein, Graceffa, & Dominguez, 2001).

Different types of actin binding proteins remodel or modify existing filaments. These include, among others, profilin and cofilin (Dos Remedios et al., 2003). Profilin catalyzes the exchange of bound ADP for ATP resulting in ATP-actin monomers which readily assemble into filaments. Cofilin binds to actin to enhance the rate of dissociation of ADP-actin monomers from the pointed end. It can also sever actin filaments creating new barbed and pointed ends (Bindschadler, Osborn, Dewey, & McGrath, 2004). Actin filaments can be organized into bundles or networks via cross-linking proteins (Tseng et al., 2005). These filaments can form stress fibers and are involved in forming lamellipodia, filopodia, or blebs (Fig.2). All of which have distinct roles in the actin cytoskeleton function (Le Clainche & Carlier, 2008). Stress fibers are higher order cytoskeletal structures composed of crosslinked actin filament bundles (Hotulainen & Lappalainen, 2006). Lamellipodia are sheet-like protrusions characterized by a branched actin network, typically observed at the leading edge of motile cells (Zimmermann & Falcke, 2014). Filopodia differ structurally from lamellipodia, they are finger-like extensions of the plasma membrane characterized by parallel arrays of F-actin generated at the tip of the filopodium (Katharina Grikscheit & Grosse, 2016). Finally, blebs are blister-like protrusions that occur at the cell surface (Charras, Hu, Coughlin, & Mitchison, 2006). The assembly and disassembly of actin filaments rapidly responds to extracellular signals and is tightly controlled (Lee & Dominguez, 2010).

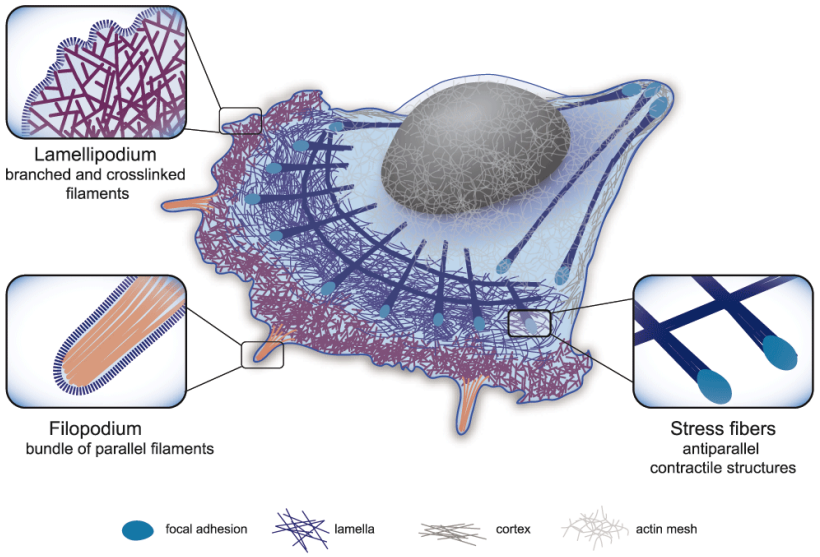

Figure 2. Cellular actin organization.

Schematic representation of actin-containing structures found in the cell. Zoomed regions highlight the specific actin organization of lamellipodium, filopodium, and stress fibers. Adapted from (Blanchoin, Letort, Ennomani, Gressin, & Théry, 2015).

1.2 Regulation of actin nucleation/polymerization

De novo actin filament formation is kinetically unfavorable and requires the involvement of one of the three major classes of actin nucleators in addition to nucleation promoting factors (NPF) (Fig.3) (Chesarone & Goode, 2009). The actin-related protein 2/3 (Arp2/3) complex and the formin homology proteins are the most commonly described nucleators. The third group, known as tandem-monomer-binding nucleators includes the Spire proteins, Cordon-bleu (Cobl), Leiomodin (Lmod-2), adenomatous polyposis coli (APC), and junction-mediating regulatory protein (JMY). While all three classes are capable of nucleating G-actin and are involved in the polymerization of actin filaments, their individual mechanisms are rather distinct (Campellone & Welch, 2010).

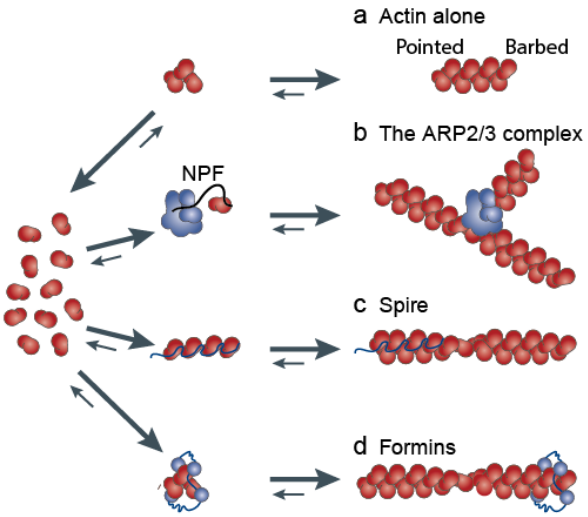

Figure 3. Different actin nucleator classes.

The spontaneous nucleation of actin to assemble into filaments is kinetically unfavorable **(a)**. Examples of the three main actin nucleators, the actin-related protein-2/3 (Arp2/3) complex, spire, and formins bypass the need for spontaneous nucleation. Each promotes nucleation by a distinct mechanism. The Arp2/3 complex mimics an actin dimer or trimer to function as a template for the initiation of a new branched actin filament **(b)**. Spire proteins interact with formin 2 to recruit actin monomers through their WH2 domain and nucleate the assembly of linear, unbranched actin filaments **(c)**. Formins promote the nucleation of unbranched filaments **(d)**. Studies indicate that they function as dimers to stabilize actin dimers or trimers to facilitate nucleation. Furthermore, they remain associated with the growing barbed ends of filaments. WH2: WASP-Homology 2, NPF: nucleation-promoting factor. Modified from (Goley & Welch, 2006)

1.2.1 The Arp2/3 complex and branched nucleation

The Arp2/3 complex was the first nucleating factor to be discovered (Machesky, Atkinson, Ampe, Vandekerckhove, & Pollard, 1994). It is composed of seven subunits: Arp2, Arp3, and ARPC1-5. It is conserved in almost all eukaryotes. Arp2/3 binds near the barbed ends of a pre-existing ‘‘mother’’ filament and forms a new ‘‘daughter’’ branch with a 70 degree angle (Rouiller et al., 2008; Volkmann et al., 2001). The Arp2/3 complex is activated by nucleation promoting factors such as WASP (Wiskott-Aldrich Syndrome protein), N-WASP (N:neuronal), WAVE/Scar (WASP family Verprolin-homologues), WASH (WASP and Scar homologue), and cortactin (Goley, Rodenbusch, Martin, & Welch, 2004). WASP, for example, exists in an auto-inhibited state until it is activated by CDC42 which binds to the GBD (GTPase binding domain), displacing the WCA domains (Erfei & Zigmond, 1999; Prehoda, Scott, Mullins, & Lim, 2000) (Fig.4). The WCA domain interacts with the Arp2/3 complex, specifically Arp2 and Arp3. This will induce a conformational change in each of the seven subunits enabling G-actin to bind to the complex. The newly nucleated daughter filament will continue to grow by polymerization (Goley & Welch, 2006).

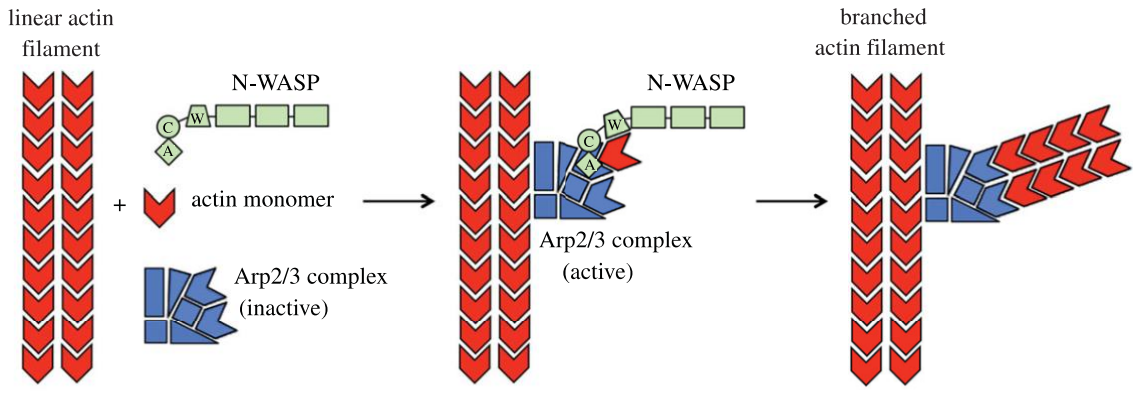

Figure 4. Arp2/3 mediated actin polymerization.

NPFs such as N-WASP mediate Arp2/3 F-actin assembly. The W region delivers actin monomers to the Arp2/3 nucleation machinery, whereas the C and A regions bind and activate the Arp2/3 complex. This leads to the assembly of a branched actin filament. Modified from (Ireton, 2013)

1.2.2 Formins and other nucleators

Formins are the largest group of actin nucleators and are highly conserved in animals, plants, and fungi. Formins are potent actin regulators which are able to directly nucleate and/or elongate actin filaments (Goode & Eck, 2007). They nucleate and polymerize actin filaments at focal adhesions at a rate of around 0.3 µm/min . Inhibiting formin protein expression results in a decreased filament elongation rate (0.1 µm/min), coupled with abnormal stress fiber morphology and an accumulation of actin binding proteins (i.e. α-actinin) (Hotulainen & Lappalainen, 2006). Formins nucleate long unbranched actin filaments (Chesarone & Goode, 2009). Furthermore, in the case of many formins (i.e. mDia1), they remain associated with the barbed end during filament elongation and presumably prevent the binding of capping proteins (Mizuno, Tanaka, Yamashiro, Narita, & Watanabe, 2018).

The tandem-monomer-binding nucleators possess repeats of G-actin binding motifs. Common to all these proteins are repeats of the actin binding motif (WASp)- homology 2 (WH2) domain. However, additional actin binding motifs may be present in the individual members. This provides variation in their mechanisms of nucleation and in the cellular functions they facilitate (Dominguez, 2016).

1.3 The formin homology protein family

There are 15 different formin protein members in mammals which can be divided phylogenetically into seven subgroups (Fig.5). The major feature of formins is the highly conserved C-terminal formin homology 2 (FH2) domain, which is essential for driving actin dynamics (Faix & Grosse, 2006). Because of their role in remodeling the actin cytoskeleton and regulating microtubule dynamics (Chesarone, DuPage, & Goode, 2010), formins are crucial for cellular processes like migration, cytokinesis, and organelle trafficking (Young & Copeland, 2010).

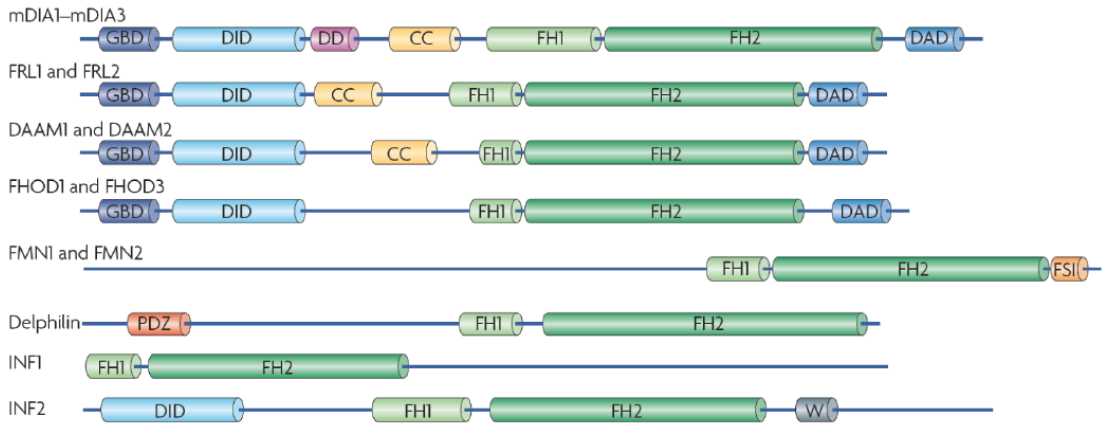

Figure 5. Domain organization of the seven mammalian formin subfamilies.

Formin subfamilies are classified based on the sequence similarity of the critical actin-nucleating FH2 domain. GBD: GTPase-Binding Domain. DID: Diaphanous Inhibitory Domain. FH1: Formin Homology 1 domain. FH2: Formin Homology 2 domain. DAD: Diaphanous Autoregulatory Domain. FRL is synonymous with FMNL. Modified from (Campellone & Welch, 2010)

1.3.1 Actin assembly by formins

The FH2 domain of formins initiates the nucleation of new actin filaments by stabilizing pre-existing actin dimers/ trimers. Two FH2 domains form an anti-parallel donut-shaped homodimer and associate with the barbed end of actin filaments (Fig.6).The current model suggests that formins processively stair-step at the end of elongating actin filaments to incorporate profilin-actin, while forming a donut-shaped structure (Courtemanche, 2018). Ena/VASP proteins support formin-mediated filament elongation by tethering the filaments near sites of active actin assembly (Breitsprecher et al., 2011). The mechanism by which the FH2 domain functions as a processive cap is not yet fully established and hence remains a working model (Goode & Eck, 2007). During the process of actin filament elongation, the dimerized FH2 domains undergo conformational changes (Fig.6). In the open conformation, one FH2 domain takes a step towards the barbed end of the filament, either before or after G-actin incorporation. After the second FH2 domain repeats this step, both FH2 domains adopt a closed conformation and remain associated with the barbed end. In several formin proteins, a proline rich FH1 domain is located N-terminally in front of the FH2 domain. The FH1 domain is able to bind profilin and hence recruit ATP-bound profilin-G-actin complexes to the FH2 domain, accelerating further polymerization at the barbed end.

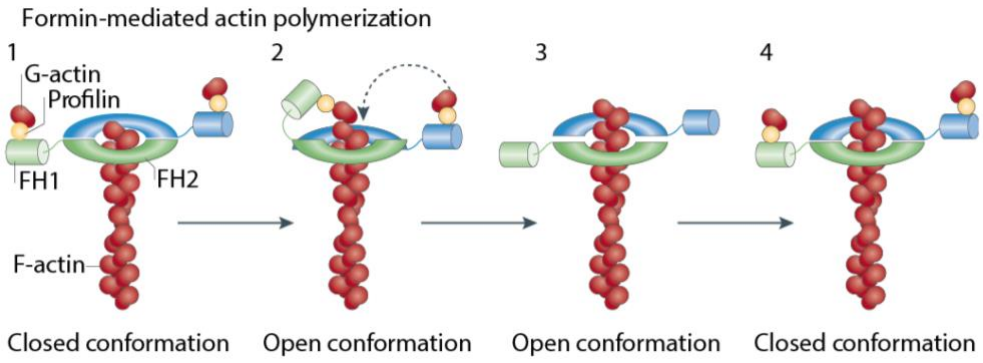

Figure 6. Formin-mediated actin filament polymerization model.

The FH2 dimer associates with the barbed end of the actin filament **(1)**. The profilin-G-actin complex can bind to the flexible FH1 domain of formin and then transfer rapidly onto the end of the growing filament. The FH2 domain steps reliably onto the new actin subunit **(2)**. The second FH2 repeats this process **(3)**. The formin closed confirmation prevents capping by other factors **(4).** Modified from (Campellone & Welch, 2010)

The ability of individual formins to nucleate actin, associate with barbed ends, or interact with profilin varies remarkably between the different formins. For example, INF2 nucleates actin, but also causes actin severing and disassembly (Chhabra & Higgs, 2006). mDia2, on the other hand binds to the barbed ends of actin filaments and promotes strong polymerization activity (Kühn & Geyer, 2014). Even though formins share a common mechanism in actin polymerization, we still find substantial differences in their actin assembly abilities (Kovar & Pollard, 2004).

1.3.2 Formin domain organization and regulation

Diaphanous-related formins (DRFs) are the prototypic formins, and are effectors of Rho family GTPases. They encompass the four mammalian families mDia, Daam, FHOD, and FMNL that share a similar domain organization (Baarlink, Brandt, & Grosse, 2010). This includes a GTPase binding domain at the N-terminus adjacent to a Diaphanous-inhibitory domain (DID) and a dimerization domain (DD). The C-terminus comprises the FH1, FH2 domain, along with the Diaphanous-autoregulatory domain (DAD) (Faix & Grosse, 2006) (Fig.5). The interaction between the DID and the DAD of DRFs results in a basal, autoinhibited state, which can be released by the binding of an active Rho GTPase to the GBD. This allows the DID to undergo a conformational change and release the DAD (Lammers, Rose, Scrima, & Wittinghofer, 2005). It is proposed that the autoinhibitory interaction of the DID and DAD sterically prevents FH2 from contacting actin (Paul & Pollard, 2009). There are also several formins which are not autoregulated, for example mammalian Delphilin, INFs, and FMNL3 (Chhabra & Higgs, 2006; Miyagi et al., 2002; Vaillant et al., 2008). In addition to Rho GTPase binding, release of

autoinhibition can also be accomplished by post-translational modifications. It has been shown that several formins are regulated via serine-threonine phosphorylation involving various kinases such as Rho-dependent protein kinase (ROCK), aurora kinase, or PKC isoenzymes (Iskratsch et al., 2013; Shimada et al., 2004; Takeya, Taniguchi, Narumiya, & Sumimoto, 2008). However, additional unknown signals might play a role in their complete activation (Fig.7).

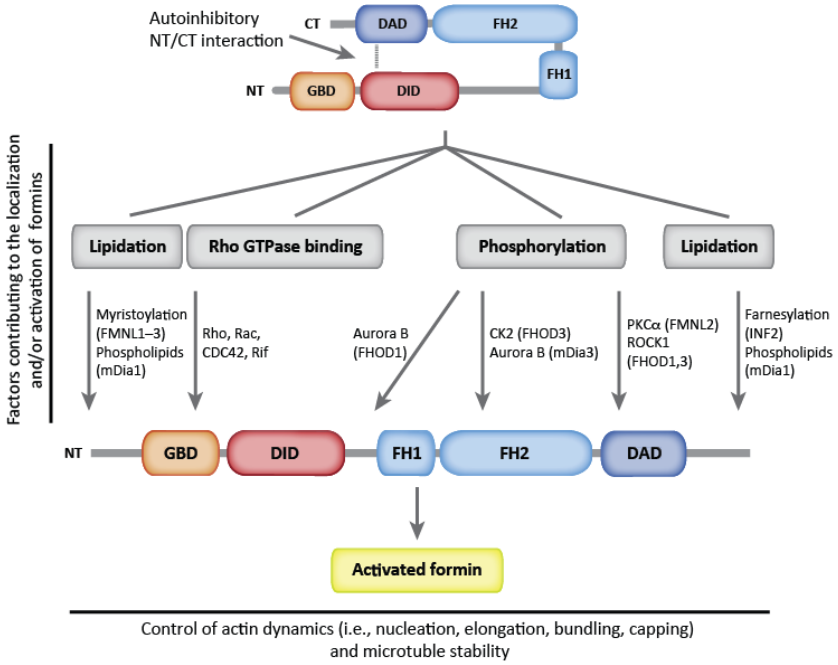

Figure 7. Domain structure and regulation of formins.

Several factors contribute to the release of autoinhibition established through the interaction of the DID and DAD domains. Active Rho GTPases such as Rho, Rac1, CDC42, or Rif trigger formin activity through release of autoinhibition by binding to the GBD domain. Additional signals such as lipidation, farnesylation, or phosphorylation have been shown to regulate activation and localization. Specific regulations for a formin or formin group are indicated in parentheses. Modified from (Katharina Grikscheit & Grosse, 2016)

1.3.3 The FRL/FMNL formin subgroup in different cell processes

The FRL/FMNL subgroup of formins share similar domain organization to diaphanous proteins (Colón-Franco, Gomez, & Billadeau, 2011) and consist of FMNL1 (FRL1), FMNL2 (FRL3) and FMNL3 (FRL2; here referred to as FMNL1-3 for consistency with recent literature). The FMNL formin family, a major focus in this thesis, is found to be co-translationally myristoylated at the N-terminus which regulates the localization of FMNL formins to the plasma and intracellular membranes (Block, Breitsprecher, Kühn, et al., 2012; Han et al., 2009; Moriya et al., 2012) and is essential for their function. N-terminal myristoylation also directly contributes to Golgi positioning of FMNL1γ, FMNL2, and FMNL3. In addition to this localization at the Golgi apparatus, both FMNL2 and 3 can be

found at various types of vesicles of different sizes. FMNL1γ regulates cellular F-actin levels required to maintain structural integrity of the Golgi complex and lysosomes (Colón-Franco et al., 2011), while FMNL2 and 3 can influence Golgi architecture and regulate anterograde transport through the Golgi apparatus (Kage, Steffen, et al., 2017). The formins FMNL2 and FMNL3 have been detected in filopodia as well as in lamellipodial structures. FMNL formin-generated filaments in lamellipodia operate in addition to Arp2/3 complex-dependent branching to strengthen these structures for promoting effective protrusion and migration (Kage, Winterhoff, et al., 2017). A critical role of FMNL2 in the assembly of junctional actin at newly forming cell-cell contacts in a 3D matrix has also been described. This activity originates downstream of Rac1 and is in line with a physical association of FMNL2 and components of the cadherin-catenin complex (K Grikscheit, Frank, Wang, & Grosse, 2015). FMNL2 was further recently implicated in β1-integrin trafficking and reported to co-localize with the early and late endosomal markers Rab4/5 and Rab7, respectively (Wang et al., 2015). Moreover, FMNL3 was also described recently to co-localize with cytoplasmic puncta of endocytic origin (Gauvin, Young, & Higgs, 2015). Based on present literature, the activity of the FMNL2 formin is found to be regulated by the Rho GTPases Cdc42, Rac1, and RhoC (Block, Breitsprecher, Kühn, et al., 2012; K Grikscheit et al., 2015; Grobe, Wü, Baarlink, Grosse, & Grikscheit, 2018; Kitzing, Wang, Pertz, Copeland, & Grosse, 2010). Furthermore, protein kinase C alpha (PKCα) phosphorylates the formin FMNL2 at a specific serine residue (Fig.8), thereby promoting its re-localization from the plasma membrane and activity (Wang et al., 2015). Importantly, FMNLs and mainly FMNL2 are upregulated in some human tumor samples and invasive cancer cell types (Péladeau, Heibein, Maltez, Copeland, & Copeland, 2016), making this group of formins particularly relevant for malignant disease.

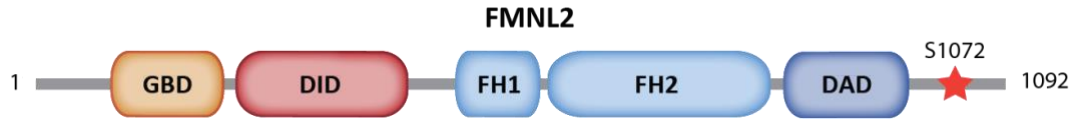

Figure 8. FMNL2 protein model showing its different domains and phosphorylation site.

1.3.3.1 FMNL formins in cancer

Few studies have implicated formins in disease pathogenesis (DeWard, Eisenmann, Matheson, & Alberts, 2010). Through their role in cytoskeletal remodeling, uncontrolled formin function may be a critical event in cancer development. Formins are required for cytokinesis through the assembly of the contractile actin ring. Loss or deregulation of formin activity interferes with cytokinesis and leads to binucleate cells (Castrillon & Wasserman, 1994; Severson, Baillie, & Bowerman, 2002). Hence, formin activity is critical for proper cell division and maintenance of genomic integrity (DeWard et al., 2010).

Formin-like 2 (FMNL2) expression was shown to be elevated in colorectal metastatic cancer cell lines compared to normal colorectal cancer cell lines. In addition, FMNL2 expression was higher in primary colorectal cancer and lymph node metastases, with the highest expression in the metastatic-derived cell lines (X. L. Zhu, Liang, & Ding, 2008a). Enhanced expression is furthermore correlated with TGFβ-induced EMT in colorectal carcinoma (Yufa Li et al., 2010). Further studies identified FMNL2 as a potential metastasis-associated gene of CRC, where FMNL2 expression profoundly increases tumor growth and metastasis *in vivo* (X.-L. Zhu et al., 2011). Additionally, several microRNAs were reported to suppress growth of colon cancer through targeting FMNL2 (Liang et al., 2013; Yan, Wang, & Qin, 2019). In other cancer models, where FMNL2 and FMNL3 are filopodial components in melanoma cell lines, depletion of FMNL2 and/or FMNL3 led to altered cell morphology and decreased migration *in vitro* (Gardberg, Heuser, Koskivuo, Koivisto, & Carpén, 2016). Increased expression of the formin family member FMNL2 functioned as a significant and independent predictor of poor outcome as measured by recurrence-free survival or melanoma-specific survival (Gardberg et al., 2016). Additionally, FMNL2 was found to drive amoeboid invasion downstream of RhoC (Kitzing et al., 2010), where RhoC has been shown to be essential for metastasis (Narumiya, Tanji, & Ishizaki, 2009). FMNL2 further promotes integrin internalization and cancer cell invasion downstream of PKCα (Wang et al., 2015).

1.4 Cancer cell invasion and metastasis

Most, if not all cancers have acquired the same set of functional capabilities during their development, albeit through various mechanisms. A key feature that distinguishes cancer cells from other cells is their ability to spread throughout the body by two related mechanisms: invasion and metastasis. These remain the most heterogeneous and poorly understood (Hanahan & Weinberg, 2011).

1.4.1 TGFβ induced invasion

One factor that is produced abundantly by stromal cells in the tumor microenvironment is transforming growth factor β (TGFβ). TGFβ is a multifunctional growth factor with a complicated dual role in tumorigenesis (David Padua et al., 2008). TGFβ is induced in response to hypoxia and inflammation and can have a protective effect on tumor cells. However, TGFβ has also been observed to drive an epithelial-to-mesenchymal transition in cancer cells, which increases their metastatic capability (Welm, 2008). Since its discovery in the early 1980s, TGFβ signaling has been increasingly recognized as a key driver in cancer (Giannelli, Villa, & Lahn, 2014). Unlike its tumor suppressor function in normal tissue, TGFβ activation causes tumor promotion in cancer tissue. This switch from tumor suppression to promotion is not well clarified, but several intrinsic and extrinsic factors seem to play important roles (N. Sun, Taguchi, & Hanash, 2016). The loss of cell polarity, acquisition of motile properties, and a mesenchymal phenotype during epithelial-mesenchymal transition (EMT) are considered crucial intrinsic changes of the tumor cells (Chaffer, San Juan, Lim, & Weinberg, 2016; Wu & Zhou, 2009).

The TGFβ signaling occurs via a canonical and a noncanonical pathway. The canonical TGFβ signaling pathway is activated when one of the three ligands (TGF-β1, TGF-β2, TGF-β3) binds to the TGF-β receptor II, heterodimerizes with the TGF-β-receptor I, and trans-phosphorylates the kinase domain of both receptors. This phosphorylation step leads to a recruitment and phosphorylation of SMAD2 and SMAD3. SMAD2 and SMAD3 form a heterotrimer with the cofactor SMAD4. This complex can enter the nucleus and bind to regions promoting the transcription of TGFβ target genes. After this, a SMAD signaling cascade is initiated and it results in nuclear translocation and gene transcription for a wide range of tumor-promoting mediators (Giannelli et al., 2014). The less-known noncanonical activation pathway is associated with several intracellular phosphorylation of proteins, such as Jun N-terminal kinase (JNK), p38 MAPK, ERK, or MEKK (Derynck & Zhang, 2003).

1.4.2 The EMT process

The formation of a primary tumor is a multi-step process, usually through a series of genetic and epigenetic changes. The determining step however, is the progress of primary carcinoma to form invasive growth and ultimately disseminate (H. Li et al., 2016). This last step is referred to as the invasion-metastasis cascade. This cascade involves

several steps including invasion, intravasation, transport, extravasation, micrometastasis, and ultimately metastasis (Tsai & Yang, 2013) (Fig.9).

The mechanism by which cancer cells acquire the ability to metastasize is a cell biological program first described in 1986, in which cells shift from one phenotypic state to the other (Greenburg & Hay, 1986). This is known as the epithelial to mesenchymal transition. This shift does not involve mutations in any genes and is hence a cell biological program. The EMT process proceeds partially and cells retain epithelial characteristics while acquiring mesenchymal ones. The EMT endows the cells with increased motility, invasive potential, and anoikis resistance (Chaffer et al., 2016; Zhang et al., 2014). This facilitates tumor metastasis which is responsible for the vast majority of cancer-related deaths. EMT is a multistep process involving many molecular and cellular changes (Tsai & Yang, 2013). Epithelial cells are highly attached to neighboring cells and are poorly motile (Macara, Guyer, Richardson, Huo, & Ahmed, 2014). During the EMT process, we notice a loss of tight junctions and epithelial adherens junctions involving E-cadherin. Loss of E-cadherin, which results in the loss of cell-cell adhesion and cell junctions is associated with the epithelial-mesenchymal transition. This allows the cells to dissociate from the primary tumor, invade surrounding tissues, and migrate to distant sites. Cells acquire a fibroblast-like shape, resulting from the rearrangement of cytoskeletal protein, particularly F-actin (Lamouille, Xu, & Derynck, 2014; Xu, Lamouille, & Derynck, 2009).

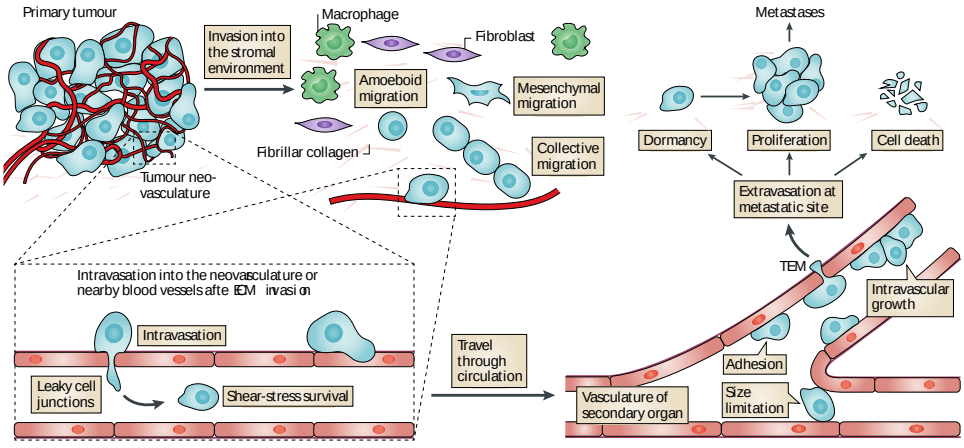

Figure 9. The EMT cascade.

For tumor cells to escape from the primary site and travel to distant organs, they must become more motile and degrade the basement membrane. This step initiates local invasion into the stromal environment. We find three forms of invasion, amoeboid, mesenchymal, and collective migration. This leads up to intravasation into nearby blood or lymphatic vessels and travel through circulation. A small subset of these, now circulating tumor cells, undergo extravasation and form

micro-metastasis. Additional signals are required for these colonies to proliferate into macro-metastasis. Otherwise, they remain dormant or undergo cell death. Modified from (Reymond, D'Água, & Ridley, 2013)

EMT is a complex and multifaceted process that involves the coordination of many factors. Adding to that complexity, is the role of the microenvironment in facilitating EMT, as this process can be initiated by hypoxia, growth factors, and inflammation (Jing, Han, Zhang, Liu, & Wei, 2011). The role and function of a specific glycoprotein secreted upon EMT initiation, will be extensively discussed next.

1.5 The ANGPTL4 glycoprotein

ANGPTL4 was first identified in the year 2000 simultaneously by three different group (P Zhu, Goh, Chin, Kersten, & Tan, 2012). It is ubiquitously expressed in humans but higher primarily in the liver. It is mainly involved in lipid and glucose metabolism. However, we now know that its function extends far beyond that with papers indicating its role in redox regulation, energy homeostasis, wound repair, angiogenesis, and most importantly tumorigenesis (P Zhu et al., 2012).

1.5.1 ANGPTL4 structure and function

The ANGPTL4 gene encodes a 406 amino acid glycoprotein. ANGPTL4 is composed of a secretory signal peptide, a coiled-coil N terminal domain and a large fibrinogen C-terminal domain (Grootaert, Van De Wiele, Verstraete, Bracke, & Vanhoecke, 2012). Both domains have different biological functions. Native full-length ANGPTL4 can form higher order structure via intermolecular disulfide bonds. The N-terminal region (nANGPTL4) is responsible for its assembly into dimeric or tetrameric structures. ANGPTL4 protein oligomerizes prior to secretion and post-translation cleavage. The oligomerization is important for its ability to inhibit LPL (Lipoprotein lipase). Cleavage is achieved by proprotein convertases at the linker region releasing the nANGPTL4 and cANGPTL4 (Fig.10) (Lei et al., 2011; P Zhu et al., 2012). The cleavage appears to be tissue specific. Recently, the cANGPTL4 protein was shown to interact with integrins β1 and β5 indicating a more complex role for ANGPTL4 (Goh et al., 2010).

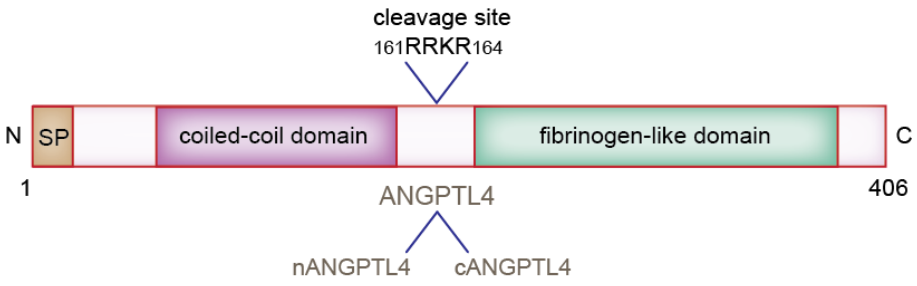

Figure 10. Schematic model of ANGPTL4 indicating the cleavage site.

ANGPTL4 expression is regulated by the nuclear hormone receptor of the PPAR family, as well as by hypoxia and fasting (P Zhu et al., 2012). TGFβ can also stimulate ANGPTL4 expression via a Smad3-signaling pathway (B. Li et al., 2017). Little is known about the relative expression of the various ANGPTL4 fragments (FL, NT, CT) in different tissue. The mechanism for such tissue dependent-expression remains unclear. Much less is known about the expression of various ANGPTL4 fragments in tumors. However, elevated ANGPTL4 expression has been revealed in up to 40 known human epithelial tumor types where the expression increased as the tumor progressed from a benign to a metastatic state (Tan, Teo, Sng, Zhu, & Tan, 2012).

1.5.2 ANGPTL4 in tumorigenesis and metastasis

A recent study has identified ANGPTL4 as a key player in redox cancer biology where it confers anoikis resistance to tumors by hijacking integrin-mediated signaling to maintain an elevated O_2-/H_2O_2 ratio. Additionally, ANGPTL4 knockdown enhanced cell apoptosis and sensitized tumor cells to drug treatment (Pengcheng Zhu et al., 2011). ANGPTL4 is also proposed to be a pro-angiogenic and pro-metastatic factor (Izraely et al., 2017; Le Jan et al., 2003). Notably, ANGPTL4 has been identified as one of the genes that can predict breast cancer to lung metastasis where TGFβ primes breast tumors for seeding of lung metastasis through ANGPTL4. TGFβ-induced ANGPTL4 enhances the retention of cancer cells in the lungs, disrupts vascular endothelial cell-cell junctions, increases the permeability of lung capillaries, and facilitates the endothelial passage of tumor cells, thus promoting the vital steps of metastasis (D Padua et al., 2008). Tumor-derived cANGPTL4 disrupts endothelial continuity by directly interacting with three novel binding partners: integrin α5β1, VE-cadherin (vascular endothelial cadherin), and claudin-5 in a sequential manner, thus facilitating metastasis (Huang et al., 2011). Hence, ANGPTL4 as a diagnostic biomarker may be an important avenue to explore when considering future therapeutic options.

2. Aim of the study

In previous work, we have discovered that Formin-like 2 (FMNL2) undergoes a post-translational modification and is phosphorylated at a specific serine residue (S1072) at its C-terminal Diaphanous-autoregulatory domain (DAD) which facilitates intramolecular autoinhibition. We identified PKC alpha as the main kinase phosphorylating FMNL2, thereby promoting its interaction with the alpha integrin tail as well as FMNL2 activity. This allows the FMNL2-integrin complex to be internalized to promote integrin recycling for invasive motility of cancer cells (Wang et al., 2015). In parallel, we showed that FMNL2 controls junctional actin dynamics in epithelial cells, where FMNL2 localizes to cell-cell contacts and interacts with the adherens junction complex (K Grikscheit et al., 2015). We therefore aimed to investigate the mechanisms by which FMNL2 may switch its actin assembly activity between an epithelial cell-cell versus a more mesenchymal cell-matrix adhesion phenotype. For this we searched for phospho-FMNL2 specific interaction partners that could be involved in harnessing FMNL2 function for the epithelial to mesenchymal transition (EMT). These studies should help to identify mechanisms of actin regulators in promoting EMT.

3. Material and Methods

3.1 Material

3.1.1 Reagents

Table 1. Reagents used.

Reagent	Manufacturer
Acetic acid	Roth
ANGPTL4 (Human) protein	Abnova
Ampicillin	AppliChem
Acrylamide (30%) – bisacrylamide (0.8%) mixture	Roth
Agar	Roth
Ammonium persulfate (APS)	Merck
ATP	Sigma-Aldrich
ASB-14	Merck
BES	Sigma-Aldrich
Bisindolylmaleimide I	Cell Signaling
Bovine serum albumin, Fraction V	Roth
Bromophenol blue	Roth
Calcium Chloride ($CaCl_2$)	Roth
Chloroform	Roth
Cholera Toxin	Sigma-Aldrich
CK-666	Sigma-Aldrich
Coomassie Brilliant Blue G250	Roth
DAPI	Sigma-Aldrich
DMEM (Dulbecco's Modified Eagle's Medium)	Capricorn
DMEM/ F12	Gibco Life Technologies
DNA 1 kb plus marker	Thermo Fischer
DNA loading dye 6x	Thermo Fischer
dNTPs	Promega
DPBS (Ca^{2+} and Mg^{2+} free)	PAA/GE Healthcare
Dimethyl sulfoxide (DMSO)	Roth
Doxycycline hyclate	Sigma-Aldrich
Dry milk, fat free	Roth
DTT (1,4-dithiothreitol)	Roth

EDTA (ethylendiamine tetraacetic acid)	Roth
Epidermal growth factor	Promo-kinase
Ethanol, absolute	Roth
Ethidium bromide	Roth
FBS (fetal bovine serum)	Invitrogen
Flag (M2) -conjugated agarose	Sigma-Aldrich
Fluorescence mounting media	DAKO
Formaldehyde (37%)	Roth
Fugene HD	Promega
Glycerol	Roth
Glycine	Roth
H_2O_2	Sigma-Aldrich
Horse serum	Invitrogen
Hydrochloric acid	Roth
Hydrocortisone	Sigma-Aldrich
Insulin	Gibco
Isopropanol	Roth
Kanamycin	Roth
Latrunculin A	ThermoFischer
Lipofectamine LTX 3000	Life Technologies
Lipofectamine RNAiMax	Life Technologies
Luminol	Sigma-Aldrich
Magnesium chloride hexahydrate	Roth
Matrigel	Corning
2-mercaptoethanol	Merck
Methanol	Roth
OptiMEM	Invitrogen
PageRuler Prestained Protein Ladder	ThermoFischer
Penicillin/Streptomycin	Capricorn
Phalloidin, Rhodamine- /AlexaFluor- conjugated	Invitrogen
Phusion Hot Start II DNA Polymerase	ThermoFischer
Protease inhibitor cocktail tablets, complete, EDTA-free	Roche
Protein A/G beads	Santa Cruz
Puromycin	Sigma-Aldrich
RNA-to-cDNA kit	ThermoFischer

SDS (sodium dodecylsulfate)	Roth
SMIFH2	Sigma-Aldrich
Sodium chloride	Roth
Sodium dodecyl sulfate (SDS)	Roth
Sodium hydroxide	Roth
SYBR-Green	Bio-Rad
T4 DNA Ligase	ThermoFischer
TEMED (N,N,N',N'-tetramethyl-ethane-1,2-diamine)	Roth
TPA (12-O-tetradecanoylphorbol-13-acetate)	Merck
Tris (tris-(hydroxymethyl)-aminomethane)	Roth
Triton X-100	Merck
TRIzol	Invitrogen
Trypsin-EDTA 0.05%	Capricorn
Tryptone	Roth
Tween-20	Roth
Yeast extract	Roth

3.1.2 Antibodies

Table 2. Primary antibodies used in this work.

Antibody	Source	Manufacturer	Application
anti-ANGPTL4	rabbit monoclonal	Sigma	1:1000 WB,IF
anti-E-cadherin	rabbit monoclonal	CST	1:1000 WB, 1:400 IF
anti-N-cadherin	rabbit monoclonal	CST	1:1000 WB
anti-Fibronectin	mouse monoclonal	Sigma	1:1000 IF
anti-FLAG-HRP	mouse monoclonal	Sigma	1:5000 WB
anti-FLAG M2	mouse monoclonal	Sigma	1:250 IF
anti-FMNL2	rabbit monoclonal	Atlas antibodies, Stockholm	1:2000 WB
anti-Golgin-97	mouse monoclonal	Invitrogen	1:1000 IF
anti-GST-HRP	mouse monoclonal	Sigma	1:5000 WB
anti-His	rabbit monoclonal	CST	1:250 WB
anti-PKCα	rabbit monoclonal	CST	1:1000 WB

anti-PKC(S)	rabbit monoclonal	CST	1:1000 WB
anti-Smad2/p-Smad2	rabbit monoclonal	CST	1:1000 WB
anti-Snail	mouse monoclonal	CST	1:1000 WB
anti-Tubulin	rabbit monoclonal	CST	1:5000 WB
anti-Vimentin	rabbit monoclonal	Abcam	1:2000 WB

Table 3. Secondary antibodies used in this work.

anti-rabbit IgG-HRP	goat	Biorad	1:5000 WB
anti-mouse IgG-HRP	sheep	GE-Healthcare	1:5000 WB

3.1.3 Kits

Table 4. Biochemical kits used in this work.

Kit	Manufacturer
NucleoBond Xtra Midi Plus	Macherey-Nagel
NucleoSpin gel and PCR clean-up	Macherey-Nagel
NucleoSpin Plasmid	Macherey-Nagel
PureLink HiPure Plasmid	Macherey-Nagel
Filter Maxiprep kit	Thermo Scientific
SuperSignal West Femto Maximum Sensitivity ECL Western Blotting Substrate	Thermo Scientific
Human ANGPTL4 Duoset ELISA	R&D Systems

3.1.4 Standard solutions and buffers

Table 5. Standard solutions and buffers used.

Solution	Composition		Remarks
2x BBS transfection buffer	BES NaCl Na_2HPO_4 dissolved in deionized water	0.05 M 0.28 M 0.0015 M	pH 6.92
ECL solution A	Tris-HCl Luminol	100 mM 2.5 mM	pH 8.5

	p-Coumaric acid	0.4 mM	
ECL solution B	Tris-HCl H_2O_2	100 mM 0.018% v/v	pH 8.5
4x Laemmli buffer	Glycerol EDTA SDS 2-mercaptoethanol Bromophenol blue Tris-HCl	28% 10 mM 5.7% 4.7 mg/ml 3.5 mg/ml 286 mM	pH 6.8
LB agar	NaCl Yeast extract Tryptone Agar dissolved in deionized water	1% 0.5% 1% 1.5%	autoclaved
LB medium	NaCl Yeast extract Tryptone dissolved in deionized water	1% 0.5% 1%	autoclaved
PBS	Na_2HPO_4 KH_2PO_4 NaCl KCl	8 mM 1.5 mM 137 mM 2.7 mM	pH 7.4
PCR sample loading buffer (6x)	Glycerol Bromophenol blue dissolved in deionised water	30% 0.25%	
SDS-PAGE running buffer	Glycine SDS Tris-HCl	192 mM 0.1% 25 mM	pH 8.3
SDS-PAGE stacking gel	Acrylamide Bisacrylamide TEMED SDS	5.9% 0.16% 14.5 µM 0.1%	pH 6.8

	Tris-HCl $(NH_4)_2S_2O_8$	0.12 M 0.15%	
TAE buffer	EDTA Tris Acetic acid dissolved in deionized water	2 mM 40 mM 20 mM	pH 8.0
TBS-DM buffer	Dry milk NaCl Tris-HCl Tween-20	5% 500 mM 20 mM 1%	pH 7.5
TBST buffer	NaCl Tris-HCl Tween-20 dissolved in deionized water	500 mM 20 mM 1%	pH 7.5
Western blot blocking solution	NaCl Tris-HCl Bovine serum albumin NaN_3 Tween-20	500 mM 20 mM 5% 0.1% 1%	pH 7.5
Western blot transfer buffer	Glycine Tris-HCl Methanol dissolved in deionized water	192 mM 25 mM 20% v/v	pH 8.5

3.1.5 Primers for qPCR and cloning

Table 6. Primers used for qPCR.

Gene	Forward primer 5´-3´	Reverse primer 5´-3´
ANGPTL4	gacccggctcacaatgtc	ccctgaggctggatttca
PRKCA	acagtgtgggtggcttgtc	tccttgaaaggcttaaagaaacc
TATA-binding	tgcacaggagccaagagtgaa	cacatcacagctccccacca

Table 7. Primers used for cloning.

Gene	Forward primer 5´-3´	Reverse primer 5´-3´
FMNL2-FLAG PLVX	ctcgagcatgggcaacgcagggagcatgg	tctagattacttgtcgtcatcgtccttgtaatccatggagcccattgttatttcggcaccatt
FMNL2-(S1072A)-FLAG PLVX	ctcgagcatgggcaacgcagggagcatgg	tctagattacttgtcgtcatcgtccttgtaatccatggagcccattgttatttcggcaccatt
ANGPTL4-FL-mCherry	gtcgactcagcggtgctccgacggccggg	gcggccgctcaggaggctgcctctgctgccat
ANGPTL4-FL-pGex	gtcgactcggacccgtgcagtccaagtcg	gcggccgctcaggaggctgcctctgctgccat
ANGPTL4-NT-pGex	gtcgactcggacccgtgcagtccaagtcg	gcggccgctcaggcaggcttggccacctcatg
ANGPTL4-CT-pGex	gtcgactcctgcccgagatggcccagccag	gcggccgctcaggaggctgcctctgctgccat

Table 8. List of Plasmids used.

Name	Details
pMD2.G	Envelope plasmid
psSPAX2	Packaging plasmid
pInd20 puro RFP	Doxycycline inducible ctrl plasmid
TRIPZ shANGPTL4 RFP	Doxycycline inducible shANG plasmid
pLVX-puro	Lentiviral expression vector with puro resistance
PWPXL	Lentiviral constitutive gene expression
pmCherry-N1	For mCherry protein fusion
ANGPTL4-V5	Expression vector
PLVX-FMNL2-FLAG	Constitutive FMNL2 expression
PLVX-FMNL2(S1072A)-FLAG	Constitutive FMNL2 expression
PWPXL FMNL2-GFP	Constitutive FMNL2 expression, Cloned by Y.Wang
PWPXL-FMNL2(S1072A)-GFP	Constitutive FMNL2 expression, Cloned by Y.Wang
pGEX	GST gene fusion vector

3.2 Constructs and cloning

PCR primers were ordered from Sigma-Aldrich. Ultra-pure water was produced by water purification and deionization system OPTIPURE Analytic (membraPure GmbH). Expression constructs were generated and sequence-verified following standard cloning procedures. FMNL2-FLAG, FMNL2 (S1072A)-FLAG, were subcloned into the PLVX vector for transduction into the MCF10A cell line. ANGPTL4-V5 was purchased from Addgene and was subcloned into the pmCherry-N1 vector (Clonetech). Constructs of the different ANGPTL4 domains ANGPTL4-FL, ANGPTL4-NT, and ANGPTL4-CT were subcloned directly into the pGEX vector to be used for protein purification.

3.2.1 Agarose gel electrophoresis

DNA samples were mixed with 10x PCR sample loading buffer and loaded to 1% agarose gels containing 10 µg/mL ethidium bromide. DNA fragments were separated on the gel in TAE buffer under constant voltage in a agarose gel chamber (Bio-Rad). The gel was later illuminated under UV light and visualized using INFINITY gel documentation system (PEQLab).

3.3 Cell culture

3.3.1 2D and 3D cell culture

HEK293T were maintained in DMEM supplemented with 10% fetal bovine serum at 37°C in a 5% CO2 environment. MCF10A cells were maintained in DMEM/F12 (Gibco Life Technologies) supplemented with 5% horse serum, 20 ng/ml epidermal growth factor, 10 μg/ml insulin, 0.5 μg/ml hydrocortisone, 100 ng/ml cholera toxin, 100 U/ml penicillin, and 100 μg/ml streptomycin at 37 °C in a 5% CO2 atmosphere as described by(Debnath, Muthuswamy, & Brugge, 2003). When needed, cells were treated with 4 ng/mL TGFβ, 200 nM TPA, or 2 µM BIM.

3.3.1 Transfection of DNA

DNA plasmids were transfected with calcium phosphate method for HEK293T cells. Briefly, plasmids were mixed with autoclaved deionized distilled water. The same volume of 2x BBS buffer was added followed by adding 1/20 volume of 2.5 M $CaCl_2$ dropwise. The transfection mixtures were incubated at room temperature for 20 min before adding to the cells dropwise. Cells were changed into fresh complete media after 3-4 hours. For transfection of MCF10A cells, Lipofectamine 3000 was used according to manufacturer's

instructions. For one 6-well, plasmids were mixed in 100 µL serum free medium. 1 µL of Lipofectamine 3000 LTX and Plus reagent was added and mixed by vortexing. After 10 min incubation at room temperature, transfection mixtures were added to the cells.

3.3.2 Transfection of siRNA

siRNAs were transfected using RNAimax following manufacturer's instructions. For one 6-well, 20 µM siRNA in the volume of 2 µL was mixed with 186 µL serum free media and 4 µL RNAimax. After 10 min incubation at room temperature, the transfection mixtures were added to cells in a total volume of 2 mL. siRNA targeting sequences:

si ctrl	5′-AATTCTCCGAACGTGTCACGT-3′
si FMNL2_7	5′-TGGGACTAGATGGCCCACTAA-3′
si ANGPTL4	5′-AUACGGAGCUACUGGUUUA-3′

3.3.3 Generating stable cell lines by virus transduction

MCF10A stable cell lines were generated by lentiviral transduction. Viruses were produced by transfecting HEK293T cells with packaging plasmid psPAX2, envelope plasmid pMD2G and expressing plasmids: PLVX-FMNL2-FLAG, PLVX-FMNL2 (S1072A)-FLAG, pWPXL-FMNL2-GFP, pWPXL-FMNL2-S1072A-GFP, pGIPZ sh ctrl RFP, pTRIPZ sh ANGPTL4_4 RFP. sh ctrl RFP was a gift from Prof. Stiewe lab 5′TGCTGTTGACAGTGAGCGATCTCGCTTGGGCGAGAGTAAGTAGTGAAGCCACAGATGTA CTTACTCTCGCCCAAGCGAGAGTGCCTACTGCCTCGGA-3′. sh ANGPTL4-RFP_4 was purchased from Dharmacon. 1 sequence out of 4 provided a knockdown of the ANGPTL4 protein. Supernatants were harvested 48 h after transfection and filtered through 0.45 µm filter. MCF10A cells were infected by the virus supernatant. 48 h after infection, cells were trypsinized and passaged. They were either FACS- sorted to maintain a homogeneously expressing population of cells or underwent selection with 2.5 µg/mL puromycin. To induce the expression of the desired protein, doxycycline (1µg/mL) was added to the medium when needed.

3.4 Analysis of protein expression from cultured cells

3.4.1 Isolation of protein from cells

Cell culture media was removed and cells were lysed by adding 200 µL Laemmli buffer to a 6-well plate. The lysates were scraped from the cell culture dish into Eppendorf tubes

and incubated at 95°C for 10 min and then centrifuged for 5 min. Extracted cell lysates were subjected to SDS-PAGE immediately or stored at -20°C.

3.4.2 SDS-PAGE and protein transfer

Proteins were separated by sodium dodecyl sulfate polyacrylamide gel electrophoresis (SDS-PAGE) using Mini-PROTEAN Tetra Cell gel system (Bio-rad). From 8% to 12% separating gels were used according to the different sizes of the proteins which were to be separated. Gels were casted and polymerized in a vertical glass space and assembled into the vertical Tetra Cell chamber following manufacturer's instructions. The chamber was filled with SDS running buffer. Cell lysates and standard pre-stained protein marker were loaded into the wells. Proteins were electrophoretically separated at constant voltage (80 V for stacking gel and 120 V for separating gel). The gels were further subjected to Coomassie blue staining or transfer.

SDS-PAGE gels and 0.45 µm nitrocellulose membranes were assembled into a Mini Trans-Blot module and then into the Mini Trans-Blot Electrophoretic Transfer Cell following manufacturer's instructions. The transfer cell chamber was filled with Western blotting transfer buffer and proteins were transferred from the gel to the membrane at constant voltage of 100 V for 50 min to 90 min. After the transfer, membranes were placed into blocking buffer and incubated for 1 h at room temperature. Different primary antibodies were diluted in the blocking buffer and incubated with the membranes on a shaker for 1 to 2 h at room temperature or overnight at 4°C. Membranes were washed 10 min each for three times with TBST and incubated with secondary antibodies in blocking buffer for 1 h at room temperature when necessary. Membranes were washed again 10 min each for three times with TBST before developing. Enhanced chemiluminescence was used to detect the horseradish peroxidase-conjugated antibodies. Films (Fuji) were exposed on top of the membrane with ECL at different time points in a dark room and developed with the developing machine. The primary and secondary antibody dilutions are listed in Table 8.

3.4.3 RNA isolation and CDNA reverse transcription

1 mL of cold TRIzol reagent was added to the cells, they were then scraped and transferred to Eppendorf tubes. 200 µL of chloroform was added before vortexing. The samples were then centrifuged for 15 min at 12000 rpm at 4°C. The transparent phase was transferred to a new Eppendorf tube. 500 µL of Isopropanol was added. After 10 min, tubes were centrifuged again for another 10 min at 12000 rpm. One final washing step was done with 1 mL of Ethanol and then the RNA was left to dry.

1 μg RNA was mixed with 1 μL of 100 μM random hexamers and heated at 65°C for 5 min following 5 min of cooling on ice for another 5 min. A reaction mixture consisting of 1 μL reverse transcriptase, 1x RT buffer, 2 μL of 10 mM dNTP mix, 1 μL RNAse inhibitor with additional water to get a total volume of 19 μL was then then added to the RNA/primer mixture and mixed. Reaction was run as the following,
10 min 25°C, 60 min 42°C, 10 min 70°C.

3.4.4 qPCR

cDNA was diluted 1:5 ,primers were designed by the online tool Universal Probe library and listed in Table 6. A 20 µl PCR reaction mixture was composed from 12.5 µl SYBR Green Mix (2x) 7 µl H2O and 0.5 µl primers in a mix (1:1). PCR was run in a 96-well Real-Time Quantitative Thermal Cycler (Biorad) under the following program:

Time	Temperature	
3 min	95°C	
10 sec	95°C	
30 sec	60°C	40 cycles
30 sec	72°C	
2 min	95°C	
30 sec	55°C	

3.4.5 ELISA

ELISA assay was performed according to the manufacturer's instructions (BioRad). Shortly, the supernatant was harvested after different treatments and diluted 1:10 and 1:40. The plate was treated with capture antibody, blocked, samples added, detection antibody, streptavidin-HRP, substrate solution. Washing was done 3x between each step except after the last one. The reaction was stopped and absorbance was read at 450 nm in the plate reader.

3.4.6 Mass spectrometry

Mass spectrometry was performed in the Max Planck institute in Bad Nauheim as a collaboration between our lab and Dr. Johannes Graumann. Briefly, immunoprecipitation of different cellular lysates was perfomed **(3.5)**, and after the last washing step, samples were snap-frozen and sent for analysis.

3.5 Immunoprecipitation

Cells were harvested 24 or 48 h after stimulation with TGFβ by scraping and lysed in lysis buffer containing 20 mM Tris-HCl (pH 7.4), 150 mM NaCl, 2 mM EDTA, 0.1% ASB-

14, and complete protease and phosphatase inhibitors. Supernatants were collected after centrifugation (20,000 rpm, 15 min at 4°C) and incubated with FLAG conjugated agarose beads (Sigma) or Protein A/G beads for 90 min at 4°C. Beads were centrifuged and washed four times with lysis buffer. 2x Laemmli buffer was added and samples were subjected to SDS-PAGE gel and Western blotting.

3.6 Protein purification

The expression plasmid was transformed into E. coli BL21 (DE3). Bacteria were cultured in LB medium at 37°C until OD=0.6 and induced with 200 μM IPTG at 22°C for 16 h. GST fusion protein was purified using Glutathione Sepharose 4B beads (GE Healthcare) as described before (Brandt et al., 2007). Briefly, bacteria were harvested by centrifugation and lysed by sonication in lysis buffer (50 mM Tris-HCl pH 8.0, 150 mM NaCl, complete protease inhibitors). After centrifugation at 13,000 rpm at 4°C for 45 min, supernatant was collected and loaded to pre-equilibrated Glutathione Sepharose 4B beads. Beads were washed three times with high-salt washing buffer (50 mM Tris-HCl pH 8.0, 500 mM NaCl) and three times with non-salt washing buffer (50 mM Tris-HCl pH 8.0) subsequently before eluting with elution buffer (50 mM Tris-HCl pH 8.0, 10 mM Glutathione reduced).

6xHis fusion protein was purified using Ni-NTA agarose beads (Qiagen). Bacteria were lysed in 1×PBS pH 7.4, 30 mM Imidazole and 1% NP-40 with complete protease inhibitors. After centrifugation, supernatant was collected and loaded to pre-equilibrated Ni-NTA beads followed by three times high salt washing (1×PBS pH 7.4, 20 mM Imidazole, 350 mM NaCl) and three times low salt washing (1×PBS pH 7.4, 20 mM Imidazole). 6xHis fusion proteins were eluted in fractions with elution buffer (1×PBS pH 7.4, 350 mM Imidazole). Fractions were loaded to SDS-PAGE gels and subjected to Coomassie blue staining to visualize the proteins of interests. Fractions with desired protein were pooled and concentrated when needed.

3.7 Immunofluorescence staining and confocal microscopy

MCF10A cells were seeded on glass bottom dishes. 24 h or 48 h after transfection/transduction, cells were washed with PBS and fixed with 8% formaldehyde for 10 min at room temperature. After washing with PBS, 0.02% Triton-X 100 in PBS was used to permeabilize the cells for 10 min. Cells were blocked with 5% BSA in PBS for 1 h at room temperature. Primary and secondary antibodies were diluted in the blocking solution and incubated with the coverslips for 1 h each with three times PBS washing

between the two steps. DAPI staining was performed for 10 min when indicated. Coverslips were then mounted on the glass slides using fluorescent mounting media.

3.8 Live cell imaging

MCF10A cells were seeded on glass bottom dishes. 24 h or 48 h after transfection, live cell imaging was performed at 37°C, in a CO_2 chamber. Images were acquired every 30 sec with a Spinning disk confocal microscope (Zeiss), using the 100×/1.4 oil objective. Drugs were applied to the cells directly at the microscope while scanning. Images were later processed with Image J software or Metamorph.

3.9 Invasion assays and image analysis

Inverted Transwell invasion assays were performed as described (Kitzing et al., 2010). Cells were seeded 48 h before the assay and stimulated with TGFβ. Upper chambers of the Transwell inserts were coated with 50 µL growth factor reduced Matrigel (BD Biosciences) and polymerized for 60 min at 37°C. The inserts were inverted allowing cell seeding (10,000 cells per inserts for MCF10A cells) and adhering on the outer bottom. After 1 h, the Transwell inserts were reverted. The upper chambers were filled with medium containing or void of TGFβ based on the condition studied. Cells were allowed to invade for 48 h before fixation, permeabilization and subsequent staining with DAPI and phalloidin 488. Confocal z-stacks of 100 µm were acquired every 5 µm for nine random imaging fields of each insert with LSM 700 confocal microscope (Zeiss), using the 40X objective and the ZEN software (Zeiss). Quantification of the invaded (more than 15 µm) and non-invaded cell number was achieved using the Image J Analyze Particle function counting the number of the nucleus. Doxycycline was added to induce the expression of certain genes when needed.

3.10 Statistical analysis

Fluorescent image processing was done using ImageJ or Metamorph. PRISM was used for all statistical tests performed.

4. Results

The re-localization of FMNL2 away from the plasma membrane after phosphorylation by PKCα (Wang et al., 2015) appears to be reminiscent of the loss or dissociation of membrane proteins, occurring during the epithelial to mesenchymal transition. Taken into consideration the critical role FMNL2 plays in cell-cell adhesion formation (K Grikscheit et al., 2015; Grobe et al., 2018), we further aimed to understand its function in the cell-matrix context.

We chose the immortalized but non-transformed MCF10A breast epithelial cell line. MCF10A cell lines express a relatively high level of FMNL2 relative to other present formins (K Grikscheit et al., 2015) and are commonly used to study the epithelial to mesenchymal transition. Through the addition of TGFβ to the cellular medium, EMT is induced in various epithelial cell lines. As previously published (Zhang et al., 2014), 4 ng/mL of hTGFβ1 solution was sufficient to successfully induce EMT in the MCF10A cell line.

4.1 TGFβ-induced epithelial to mesenchymal transition in MCF10A cells

To determine whether stimulation with 4 ng/mL of TGFβ solution is effective, we tested this concentration in 2D and 3D cell culture accordingly. We could notice a drastic alteration in cellular morphology following exposure to TGFβ. Microscopic examination revealed that the untreated cells display the cuboidal appearance characteristic of epithelial cells in 2D culture. The untreated cells in 3D culture also maintained the typical acini structure known for epithelial cells grown in Matrigel over time. Exposure to TGFβ in 2D induced a phenotypic change where cells appeared elongated and spindle-like displaying abundant actin stress fibers. Whereas in 3D, the acini structures were lost and replaced by a flat spread out structure (Fig.11). The phenotypic change in the differentiation state was evident within 24-48 hr.

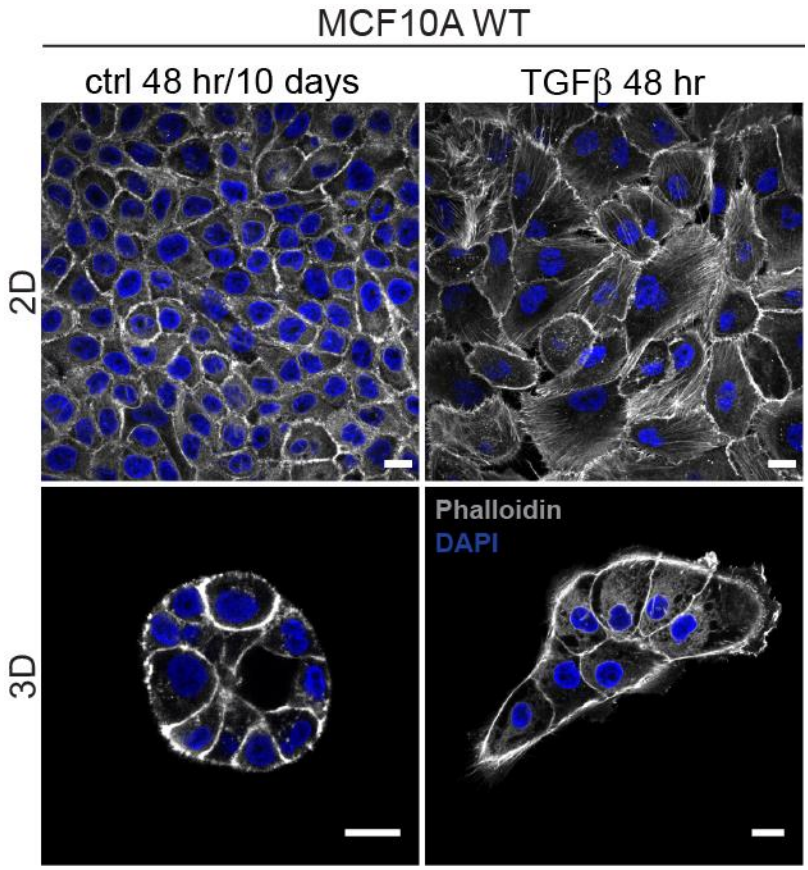

Figure 11. TGFβ stimulation of MCF10A cells in 2D and 3D cell culture.

2D culture: MCF10A cells were cultured for 48 hr in the presence or absence of 4 ng/mL of TGFβ then fixed and stained with phalloidin and DAPI. 3D culture: MCF10A cells were seeded in Matrigel and cultured for 10 days. TGFβ was added to the medium on the last two days. Cells were then fixed and stained with phalloidin and DAPI. Scale bar, 15 μm.

To verify the induction of the epithelial to mesenchymal differentiation in these epithelial cells, we tested whether the change in morphology correlated with the disappearance of epithelial markers and appearance of mesenchymal markers. We examined the expression of E-cadherin and the characteristic pattern of actin fibers using immunofluorescence. Over the time course of five days, we could see a decrease in the intensity of the E-cadherin staining, mainly at the cell-cell contact areas. We also observed the remodeling of actin filaments from cortical rings to abundant ventral stress fibers (Fig.12A). On the transcriptional program level, we saw an upregulation of the typical N-cadherin, Vimentin, and Snail markers, and a downregulation of E-cadherin (Fig.12B).

4.1.1 TGFβ-induced epithelial mesenchymal transition in MCF10A WT cells.

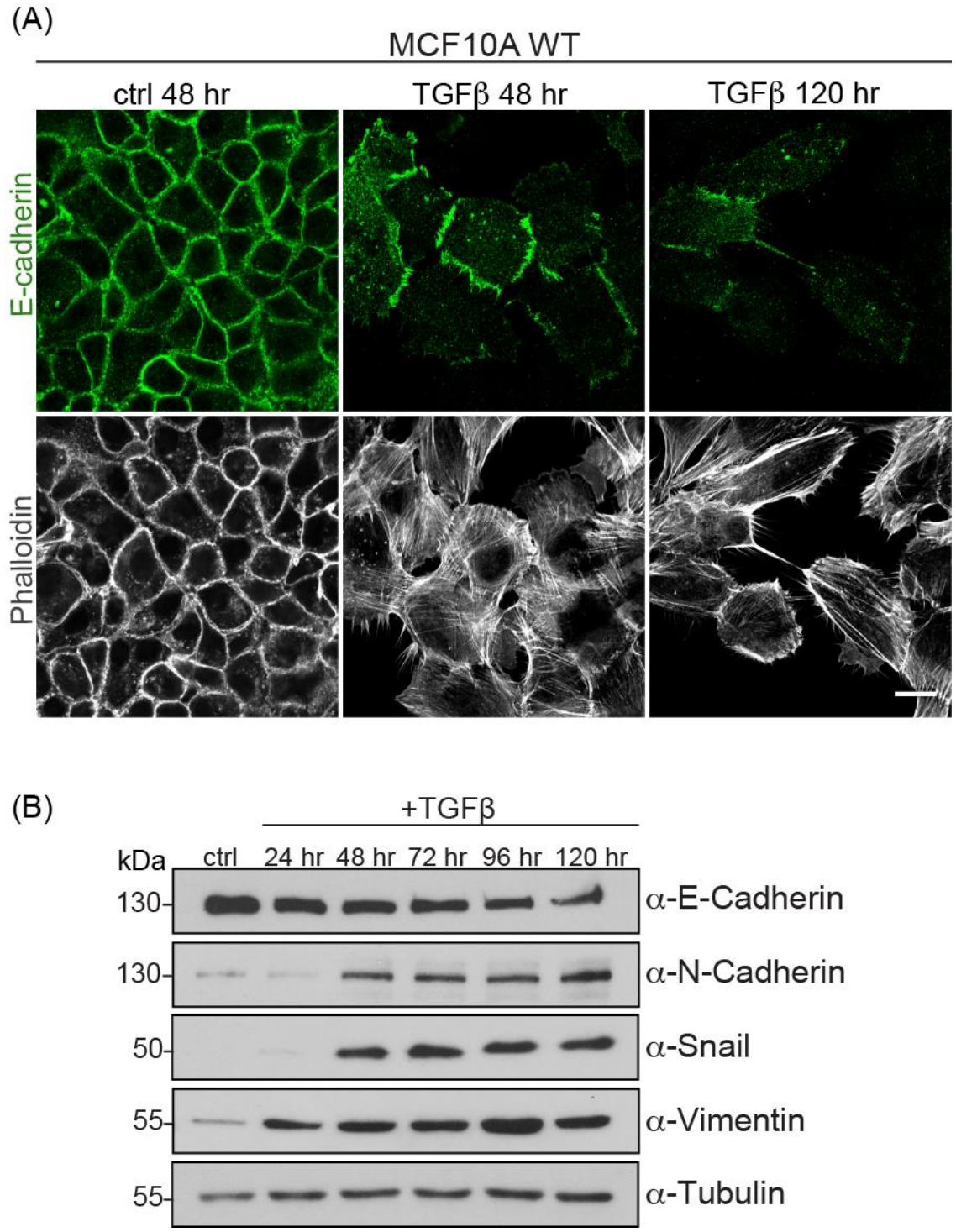

Figure 12. TGFβ-induced epithelial mesenchymal transition in MCF10A WT cells.

(A) MCF10A cells were stained for E-cadherin and actin before and after TGFβ stimulation (48 hr, 120 hr) to visualize cytoskeletal and cell-cell contact changes accompanying EMT. Scale bar, 20 μm. **(B)** MCF10A cells were stimulated with TGFβ (4 ng/mL) and samples were collected every 24 hr. Lysates were blotted against known EMT markers.

4.1.2 TGFβ-induced epithelial mesenchymal transition in MCF10A FMNL2 KO cells.

To check if FMNL2 activity is necessary for EMT induction on the transcriptional level, we utilized the MCF10A FMNL2 KO cell line. Cells were stimulated with TGFβ, fixed and stained (Fig.13A). The lysates were blotted against the previously used EMT markers (Fig.13B). We observe the same trend as with the MCF10A WT cells and conclude that FMNL2 KO cells undergo EMT as well.

To test whether the proximal step of TGFβ signaling was affected in the knockout cell line we probed for phosphorylated Smad2 and total Smad. Phosphorylated Smad2, an initial effector of the activated TGFβ receptor, forms a complex with other Smad proteins and translocates to the nucleus to complex with transcription regulators repressing or activating target genes such as E-cadherin and Snail (Lamouille et al., 2014). We could notice the expected gradual increase in p-Smad2 following the addition of TGFβ in both WT and knockout cell lines. Total Smad was unchanged in the absence or presence of TGFβ (Fig.13C). Hence, the initial transcriptional EMT program is not affected upon FMNL2 knockout.

4.2 TGFβ-induced PKC upregulation in MCF10A cells

Previous experiments to study the role of PKCs in FMNL2 regulation were performed in HeLa cells which express a high level of PKCα, the major kinase responsible for FMNL2 phosphorylation. The phorbol ester TPA (12-O-Tetradecanoylphorbol-13-acetate) was used as a stimulant to induce the phosphorylation of FMNL2 and further downstream effects. TPA activates PKC by binding to its regulatory domain (Steinberg, 2008).

We compared HeLa and MCF10A lysates after stimulation with 200 nM of TPA for 20 min and could observe that MCF10A cells only express a traceable amount of PKCα. However, we could still notice an increase in expression of PKCα upon stimulation with TPA (Fig.14A). To validate if TGFβ leads to the same effect, we stimulated MCF10A cells with 4 ng/mL TGFβ for 24 and 48 hours and could indeed see an increase in protein expression (Fig.14B). This was quantified by measuring band intensity relative to tubulin (Fig.14C) and validated through qPCR (Fig.14D).

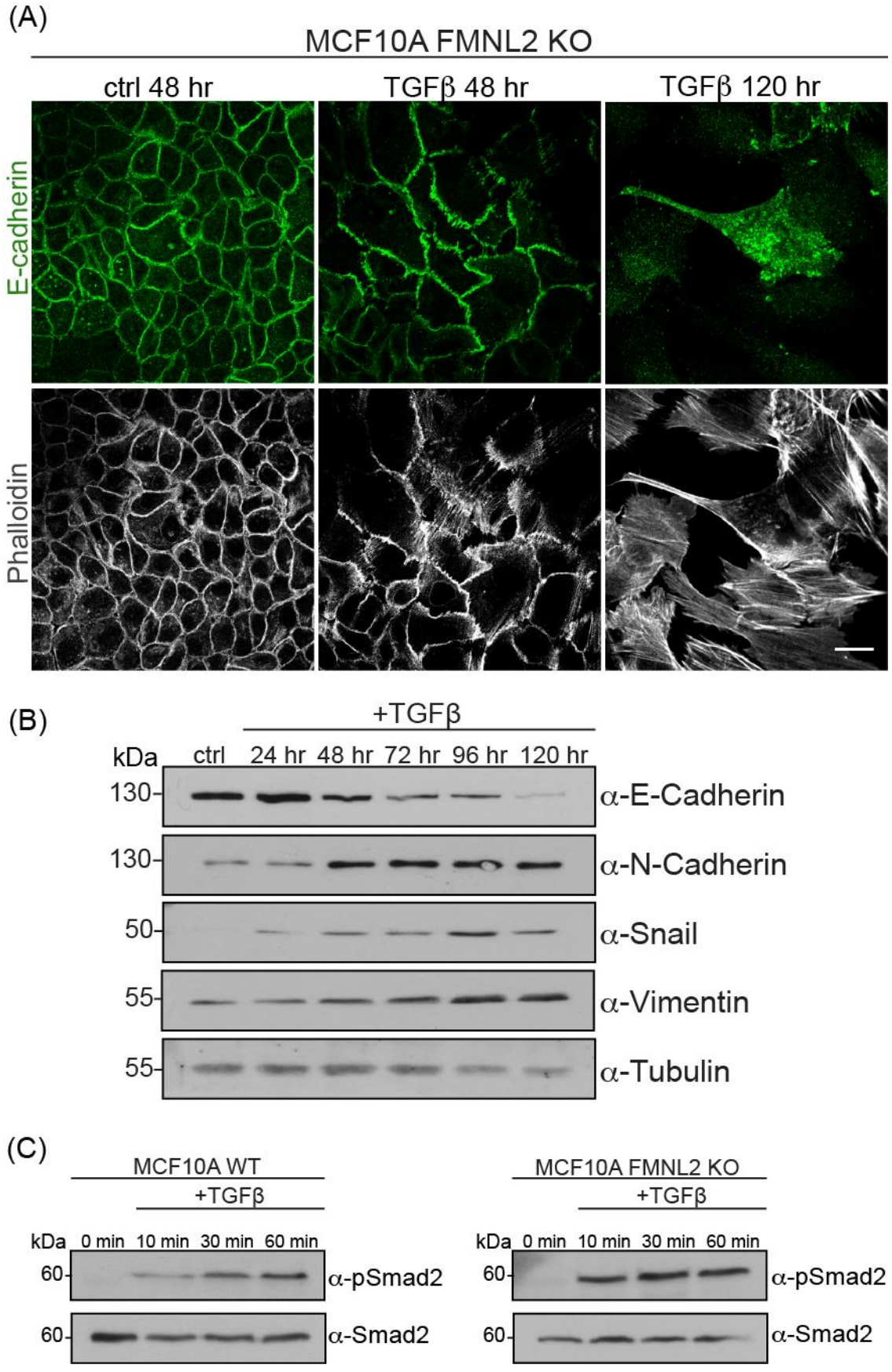
(A)
MCF10A FMNL2 KO
ctrl 48 hr
TGFβ 48 hr
TGFβ 120 hr
E-cadherin
Phalloidin
(B)
+TGFβ
kDa
ctrl
24 hr
48 hr
72 hr
96 hr
120 hr
130
α-E-Cadherin
130
α-N-Cadherin
50
α-Snail
55
α-Vimentin
55
α-Tubulin
(C)
MCF10A WT
+TGFβ
MCF10A FMNL2 KO
+TGFβ
kDa
0 min
10 min
30 min
60 min
60
α-pSmad2
60
α-Smad2
kDa
0 min
10 min
30 min
60 min
60
α-pSmad2
60
α-Smad2

Figure 13. TGFβ-induced epithelial mesenchymal transition in MCF10A FMNL2 KO cells.

(A) MCF10A cells were stained for E-cadherin and actin before and after TGFβ stimulation (48 hr, 120 hr) to visualize cytoskeletal and cell-cell contact changes accompanying EMT. Scale bar, 20 μm. **(B)** MCF10A cells were stimulated with TGFβ (4 ng/mL) and samples were collected every 24 hr. Lysates were blotted against known EMT markers. **(C)** Immunoblots of lysates from MCF10A WT and MCF10A FMNL2 KO cells maintained for different times in the absence or presence of TGFβ (4 ng/mL), probed for phosphorylated Smad2 (pSmad2) and total Smad2.

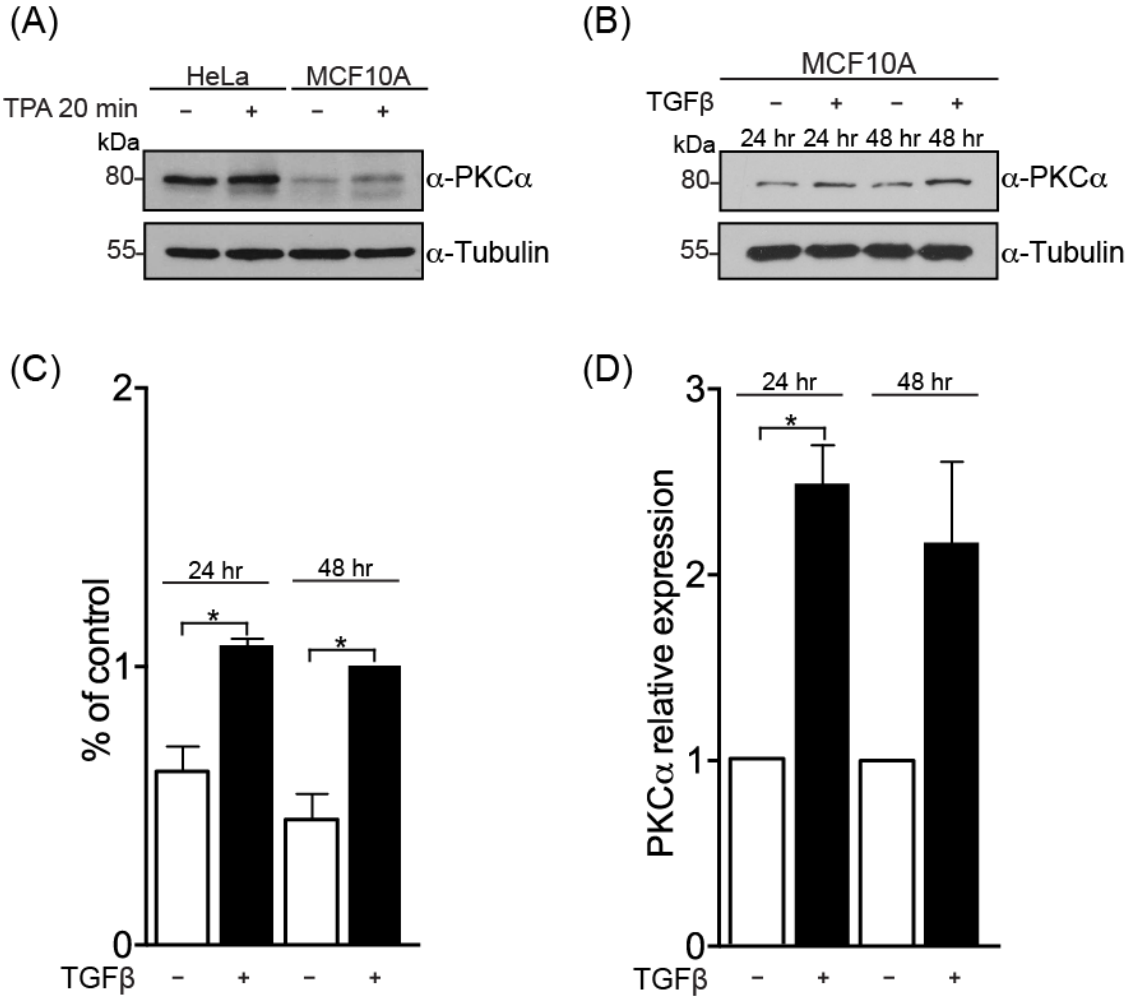

Figure 14. TGFβ-induced PKCα upregulation in MCF10A WT cells.

(A) Lysates from TPA (200 nM) stimulated HeLa and MCF10A cells were collected and compared for PKCα expression. **(B)** Lysates from TGFβ stimulated and non-stimulated MCF10A WT cells (24 hr, 48 hr) were collected and analyzed for PKCα expression followed by band intensity quantification in **(C)** (ratio of PKC/tubulin). **(D)** Relative PKCα mRNA levels after TGFβ stimulation of MCF10A cells (24 hr, 48 hr). Data is expressed as mean ± SEM. n=2. Student's t-test was performed for statistical analysis in **(C)** & **(D)***p< 0.05.

4.3 TGFβ-induced FMNL2 phosphorylation downstream of PKCα

Next, we aimed to check if TGFβ stimulation also results in the phosphorylation of FMNL2 at the aforementioned serine residue (S1072A). To guarantee a rapid and efficient immunoprecipitation of FMNL2 from MCF10A cells, all required FMNL2 constructs were cloned with a C-terminal FLAG tag to avoid any mis-localization issues since N-terminal myristoylation is required for proper localization of FMNLs (Moriya et al., 2012). They were then transduced into the MCF10A FMNL2 KO cell line. The constructs were checked for proper expression and localization (Fig.15A).

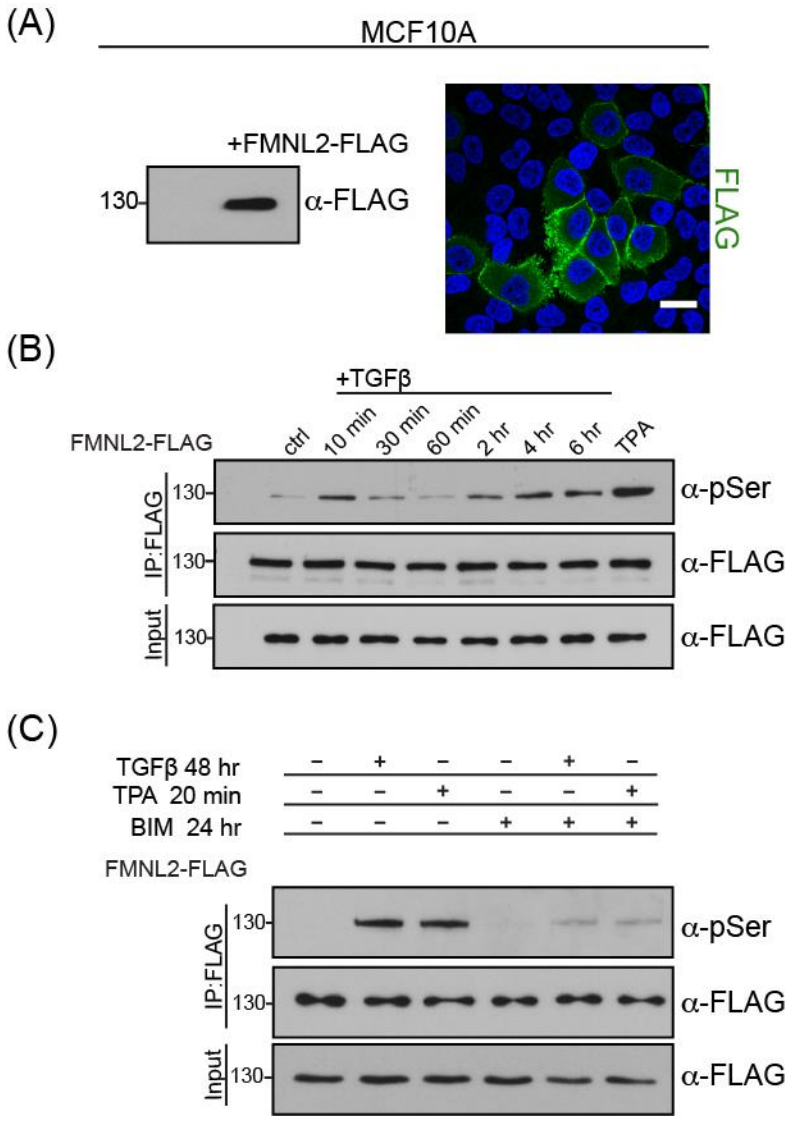

Figure 15. TGFβ promotes PKC-dependent phosphorylation of FMNL2.

(A) MCF10A cells were transduced with FMNL2-FLAG construct and the proper expression and localization was verified by an anti-FLAG immunoblot and immunofluorescent staining. Scale bar, 20 μm. **(B)** Immunoprecipitation of MCF10A FMNL2 KO cell lysates stably expressing FMNL2-FLAG at different timepoints after stimulation with 4 ng/mL TGFβ. An antibody specifically recognizing phospho-(Ser) PKC substrate was used to detect phosphorylated FMNL2. **(C)**

Immunoprecipitation of MCF10A FMNL2 KO cell lysates stably expressing FMNL2-FLAG after stimulation with 4 ng/mL TGFβ, 200 nM TPA, or 2 μM BIM respectively.

Following TGFβ stimulation, FMNL2 could be phosphorylated with a rapid increase. The phosphorylation event was evident within 10 min, level decreased shortly, then recovered after 2 hr (Fig.15B). Phosphorylation could also be detected at later timepoints (24, 48, and 72 hr, data not shown). Importantly, phosphorylation was diminished upon BIM (bisindolylmaleimide) treatment (Fig.15C) identical to the effect seen with TPA + BIM. This indicates the involvement of PKCs in phosphorylating FMNL2 downstream of TGFβ, since BIM acts as an ATP competitive inhibitor and binds the kinase domain of PKCs (Grodsky et al., 2006).

4.4 Functional analysis of FMNL2 and ANGPTL4

4.4.1 ANGPTL4 as a novel TGFβ-induced FMNL2 interaction partner

To search for additional factors involved in this pathway, we used mass spectrometry to identify FMNL2 interaction partners during TGFβ-induced EMT. We immunoprecipitated FMNL2-FLAG with or without TGFβ stimulation and the samples were sent for analysis. We observed a single significant hit, the matricellular protein Angiopoietin-like 4 (henceforth ANGPTL4) (Fig.16A). The result was confirmed by immunoprecipitating FMNL2-FLAG and blotting against endogenous ANGPTL4. Noticeably, the non-phosphorylatable mutant of FMNL2 did not interact with endogenous ANGPTL4 (Fig16.B). Hence, we conclude that the phosphorylation of FMNL2 is required for its interaction with ANGPTL4. A point mutation of the Ser residue into Ala (S1072A) to destroy the phosphorylation was introduced. The mutant S1072A could not be detected by the phospho-Ser antibody in all treatments (Wang et al., 2015).

To determine the existence of a direct interaction between FMNL2 and ANGPTL4, we purified the NT and CT of FMNL2 in addition to ANGPTL4-FL, NT, and CT. Based on the GST-pulldown results, we could detect a direct interaction between ANGPTL4-FL and both the NT and CT of FMNL2, while only ANGPTL4-NT showed this interaction (Fig.16C). We questioned the whereabouts of this interaction and used two different predictive tools (TMpred,TMHMM), to determine the exact structure of the ANGPTL4 protein (Fig.17 A,B). Both tools predicted a transmembrane domain in the N-terminus of ANGPTL4 between amino acid residues 17 and 33 following the signal peptide. Hence, it is feasible to assume that the interaction between FMNL2 and ANGPTL4 could be at cellular membranes.

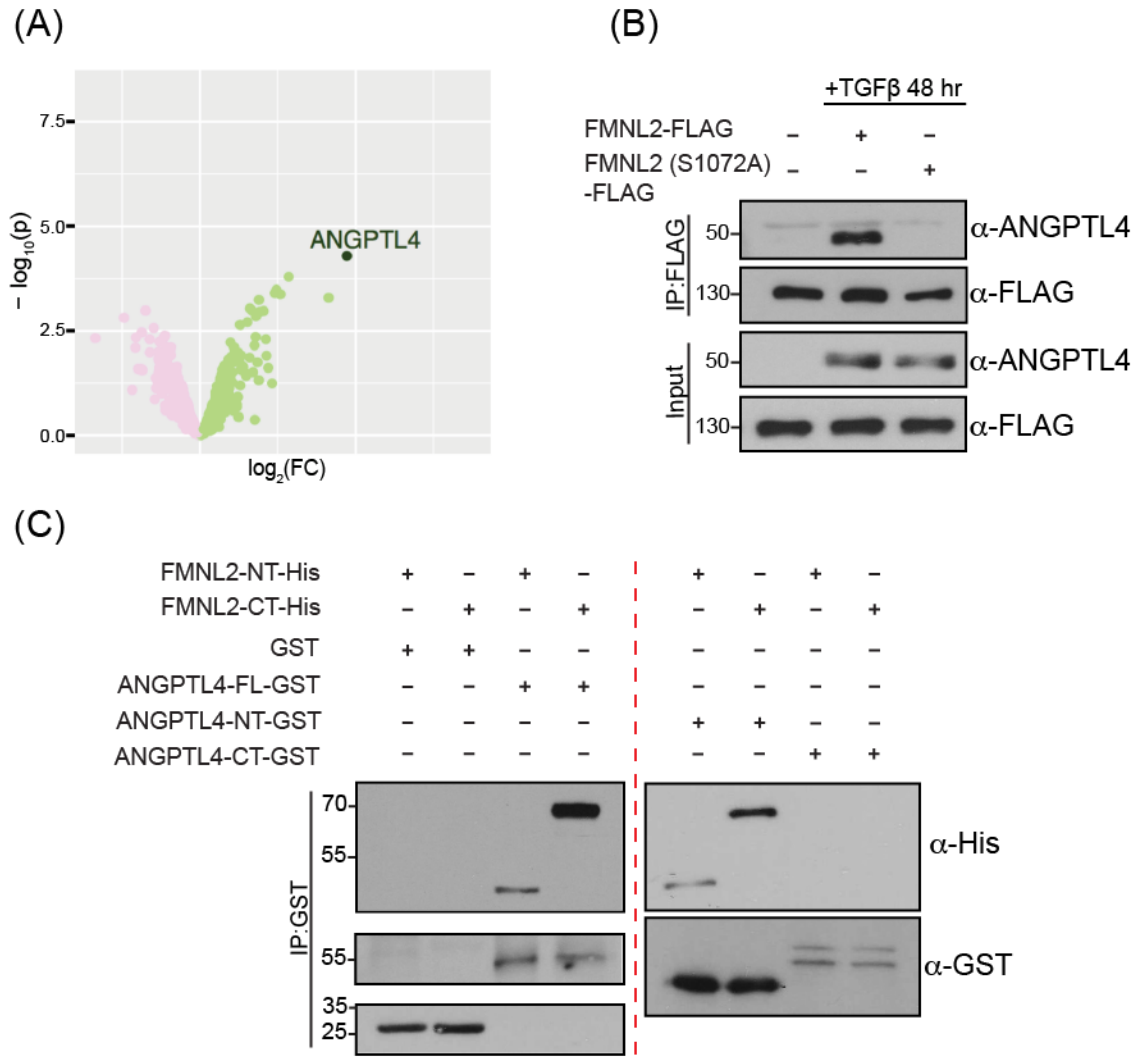

Figure 16. TGFβ-induced interaction of FMNL2 with ANGPTL4.

(A) Mass spectrometry was performed after FLAG immunoprecipitation to determine possible interaction partners of FMNL2 (ctrl v.s. TGFβ stimulation). The volcano plot summarizes the differential expression analysis. The strongest candidate is labeled. **(B)** Immunoprecipitation of MCF10A FMNL2 KO cells stably expressing FMNL2-FLAG or FMNL2 (S1072A)-FLAG with/without TGFβ stimulation (4 ng/mL) for 48 hr. Endogenous ANGPTL4 is detected. **(C)** GST-pulldown assay showcasing the interaction between GST tagged ANGPTL4 domain (FL,NT,CT) and His tagged FMNL2 (NT,CT).

4.4.2 ANGPTL4 domain organization

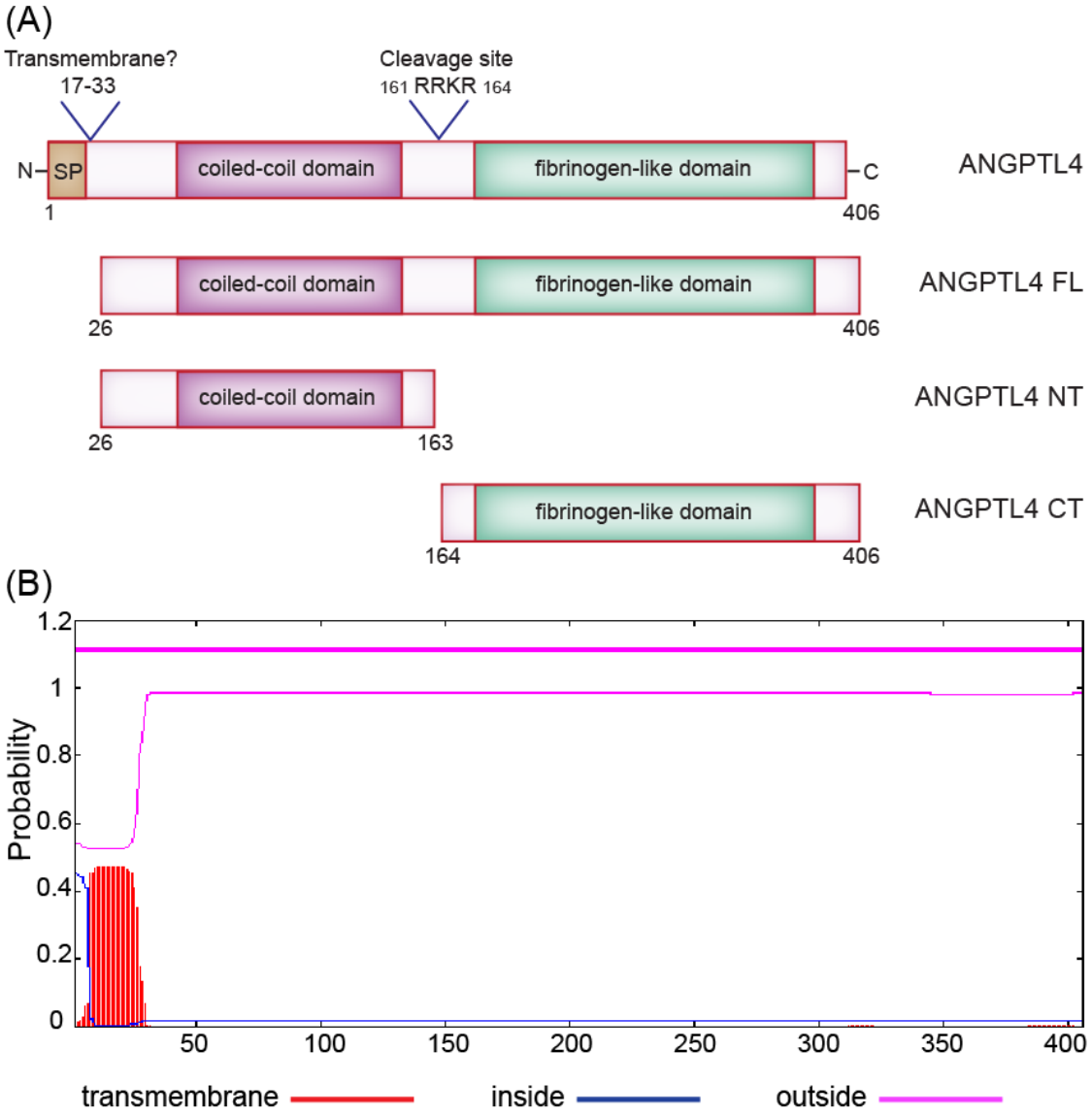

Figure 17. Schematic representation of the ANGPTL4 protein and its putative transmembrane domain.

(A) Full length ANGPTL4 and the three different constructs used for protein purification. **(B)** Probability plot for a predicted transmembrane region in ANGPTL4 by TMHMM software.

4.4.3 ANGPTL4 secretion requires FMNL2

ANGPTL4 is secreted in response to TGFβ stimulation (D Padua et al., 2008). We next determined its secretion level using an ELISA assay. We compared ANGPTL4 concentration in the presence and absence of TGFβ stimulation (24 hr /48 hr) and whether the knockout or modification of FMNL2 had an effect on its secretion. Depicted are the ELISA results after 48 hr of stimulation (Fig.18A).

The results reflect that ANGPTL4 is secreted in high concentrations reaching 600 ng/mL after TGFβ stimulation for 48 hr. Knockout of FMNL2 significantly reduces the secreted concentration to around 160 ng/mL. While re-introducing FMNL2-FLAG in the knockout cell line managed to rescue the secretion levels back to 500 ng/mL, re-introducing the phospho-mutant showed a similar result to the knockout cell line with low levels around 150 ng/mL. Without TGFβ stimulation, ANGPTL4 secretion appeared to be stagnant with minimal levels ranging around 50 ng/mL (Fig.18A). The cellular lysates were blotted against ANGPTL4 and a loading control (Fig.18B).

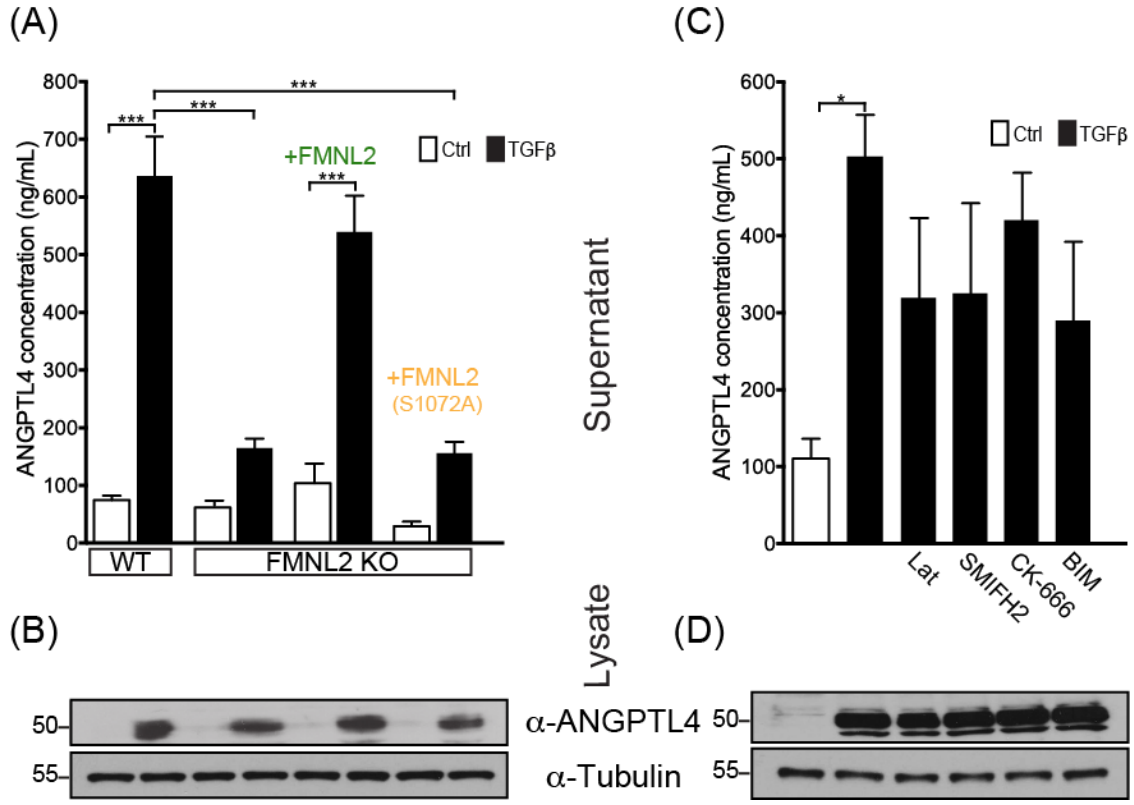

Figure 18. TGFβ targets FMNL2 for ANGPTL4 secretion.

(A) MCF10A cell lines were treated with TGFβ for 48 hr followed by supernatant collection and an ELISA assay to determine ANGPTL4 concentration. **(B)** The cellular lysates were also collected and blotted against ANGPTL4 and tubulin as a loading control. **(C)** MCF10A WT cells were pre-treated with TGFβ for 24 hr followed by 48 hr of the respective inhibitor treatment and an ELISA assay. Working concentrations: Latrunculin B: 500 nM, SMIFH2: 10 μM, CK666: 25 mM, BIM: 2 mM. **(D)** The cellular lysates were collected and blotted against ANGPTL4 and tubulin as a loading control. n=4, One-way ANOVA was performed to determine significance.*p<0.05 ***p<0.001.

Next, we tested different inhibitors acting on G-actin (Latrunculin), Formins (SMIFH2), Arp2/3 complex (CK-666), or PKC (BIM) to see their influence on ANGPTL4 secretion. Cells were first stimulated for 24 hr with TGFβ to initiate the transition and then the different indicated inhibitors were added for 48 hr, followed by supernatant collection.

Adding TGFβ and the inhibitors simultaneously had no effect (data not shown). We saw a minor but no significant decrease with Latrunculin, SMIFH2, and BIM (Fig.18C). The cellular lysates were blotted against ANGPTL4 and a loading control (Fig.18D).

4.5 Subcellular localization of FMNL2 and ANGPTL4 in MCF10A cells

To understand the relationship of FMNL2 and ANGPTL4 with intracellular structures and the possible cellular functions, we visualized ANGPTL4 on Fibronectin or in the Golgi apparatus after TGFβ stimulation (Fig.19A). ANGPTL4 still present in the Golgi, is considered to be non-secreted while secreted ANGPTL4 localizes on Fibronectin in the extracellular matrix.

4.5.1 Fixed-cell imaging of FMNL2 and ANGPTL4 in MCF10A cells

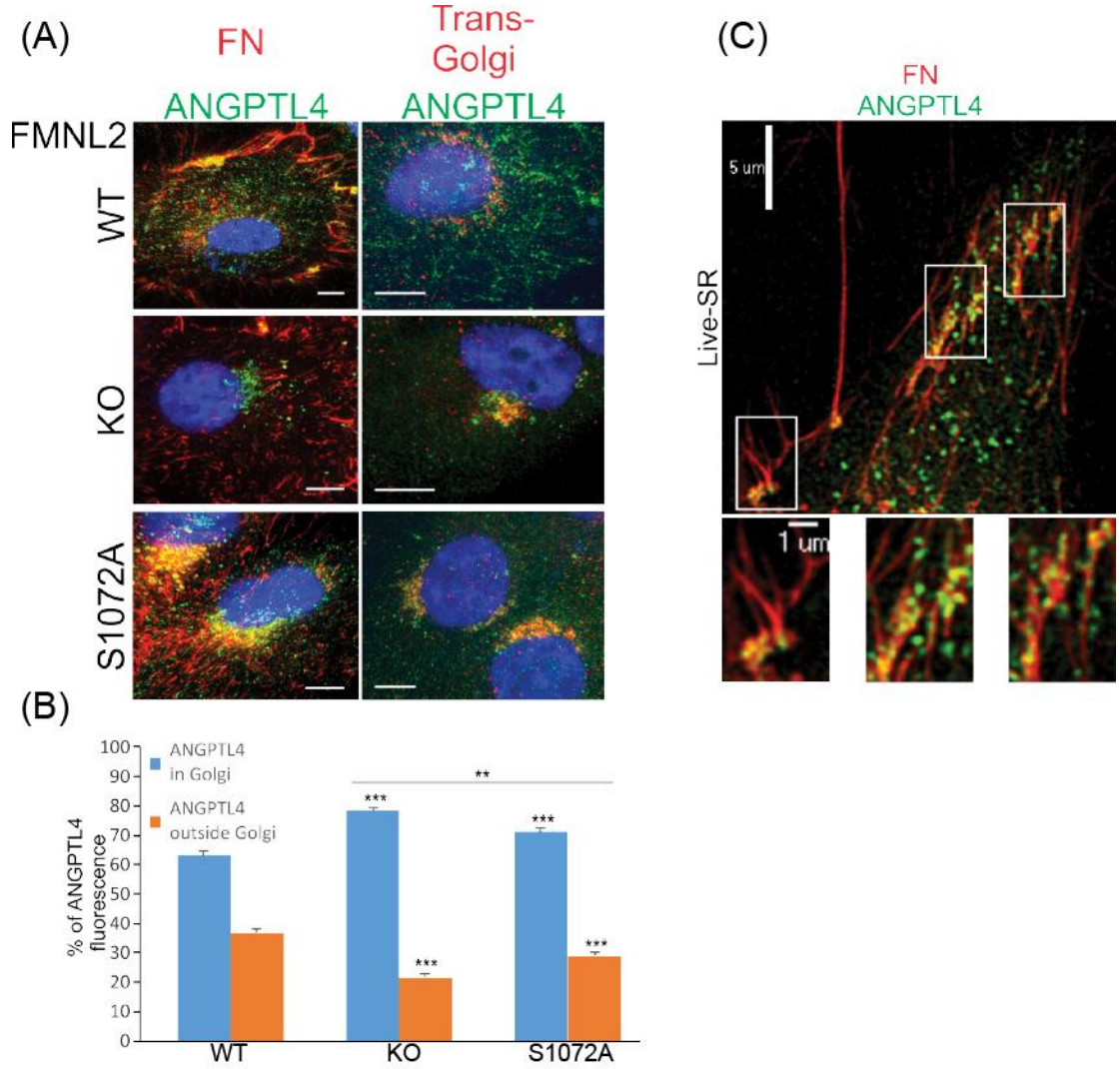

Figure 19. TGFβ-induced FMNL2 and ANGPTL4 localization in cellular structures .

(A) Extracellular (secreted) ANGPTL4 was stained and compared to intracellular (non-secreted) ANGPTL4 present in the Golgi after 48 hr of TGFβ stimulation (4 ng/mL). The differences between the three different WT, FMNL2 KO, and FMNL2 (S1072A) cell lines were assessed. Scale bar,10μm. **(B)** % of fluorescence in **(A)** was quantified and evaluated between the three different cell lines by Dr. Carsten Schwan. One-way ANOVA was performed to determine significance. **p <0.01 ***p <0.001. **(C)** High resolution microscopy visualizing secreted ANGPTL4 on Fibronectin. The three lower images represent zoom ins of the three respective drawn boxes.

We compared the differences in secretion between the WT, KO, and phospho-mutant expressing cell lines. From comparing % of fluorescence, we find less secreted ANGPTL4 (outside the Golgi) in the KO and S1072A cell lines (Fig.19B). We also notice more ANGPTL4 sequestered in the Golgi in the KO and S1072A cell lines. This indicates a possible secretion disadvantage due to the loss of functional phosphorylated FMNL2. This further confirms our previous ELISA results and that FMNL2 is required for ANGPTL4 secretion following TGFβ stimulation. To pinpoint the position of secreted ANGPTL4 in the extracellular matrix after TGFβ stimulation, we utilized high resolution microscopy and stained both ANGPTL4 and fibronectin. ANGPTL4 decorated fibronectin at cell edges, and was distributed in the extracellular matrix (Fig.19C).

4.5.2 Live-cell imaging of FMNL2 and ANGPTL4 in MCF10A cells

Finally, ANGPTL4-mCherry was transfected in the MCF10A FMNL2-GFP cell line for the live visualization of this process. Cells were stimulated with a higher dose of TGFβ (40 ng/mL) and then imaged on the next day to monitor any co-localization events occurring between FMNL2 and ANGPTL4 (Fig.20A). We could successfully observe a transient localization of FMNL2 with ANGPTL4 at certain timepoints indicated with arrows (Fig. 20B).

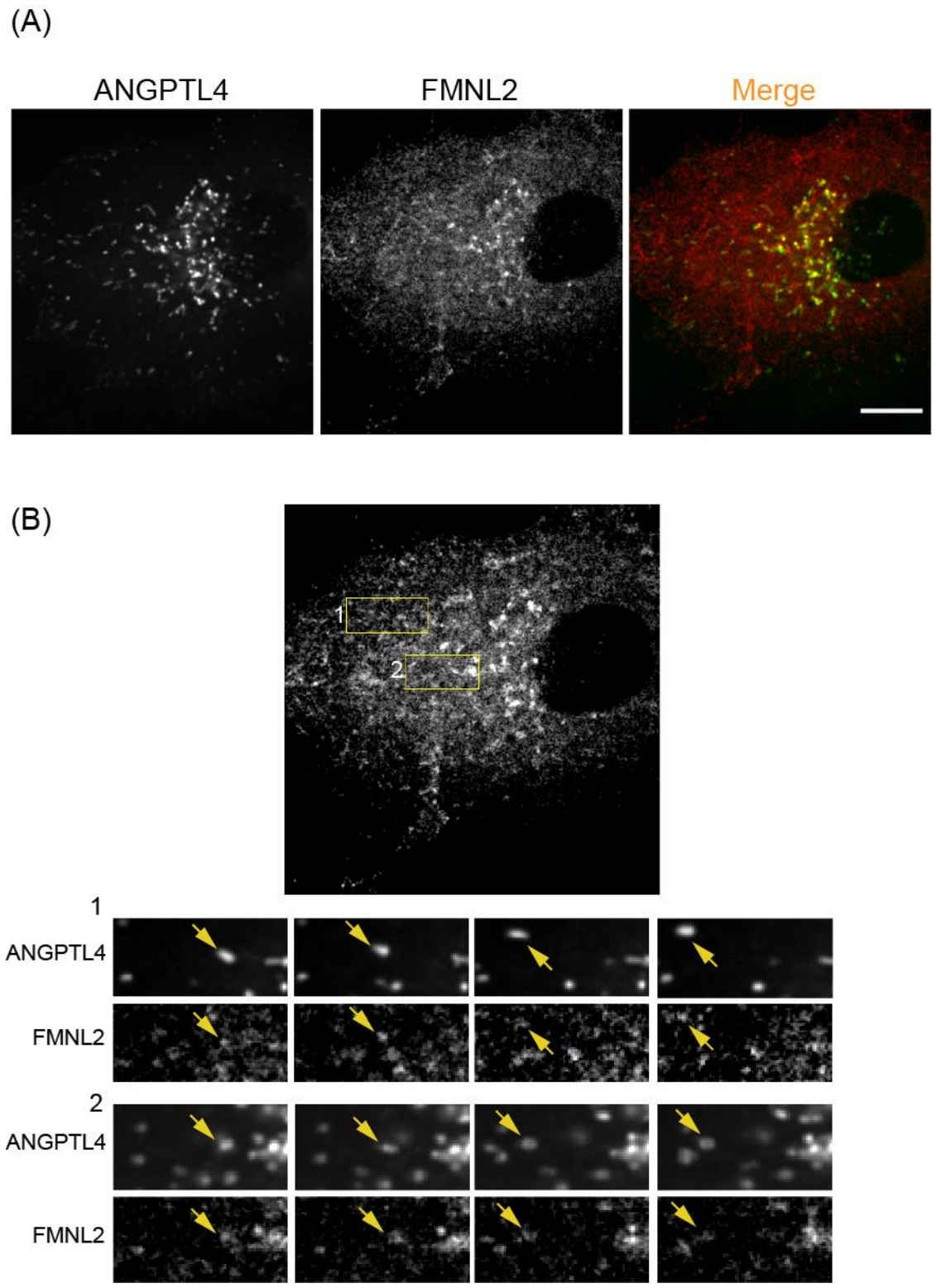

Figure 20. TGFβ-induced FMNL2 and ANGPTL4 co-localization.

(A) MCF10A-FMNL2-GFP cells were transfected with ANGPTL4-mCherry and stimulated with 40 ng/mL TGFβ on the next day. Cells were imaged after 24 hr of stimulation using spinning disk confocal microscopy to monitor FMNL2 and ANGPTL4 trafficking. Scale bar,10μm. **(B)** Zoom ins of two different regions pinpointing FMNL2 and ANGPTL4 co-localization.

4.6 FMNL2 and ANGPTL4 determine cell-cell contact integrity

4.6.1 Knockdown of ANGPTL4 in MCF10A WT cells

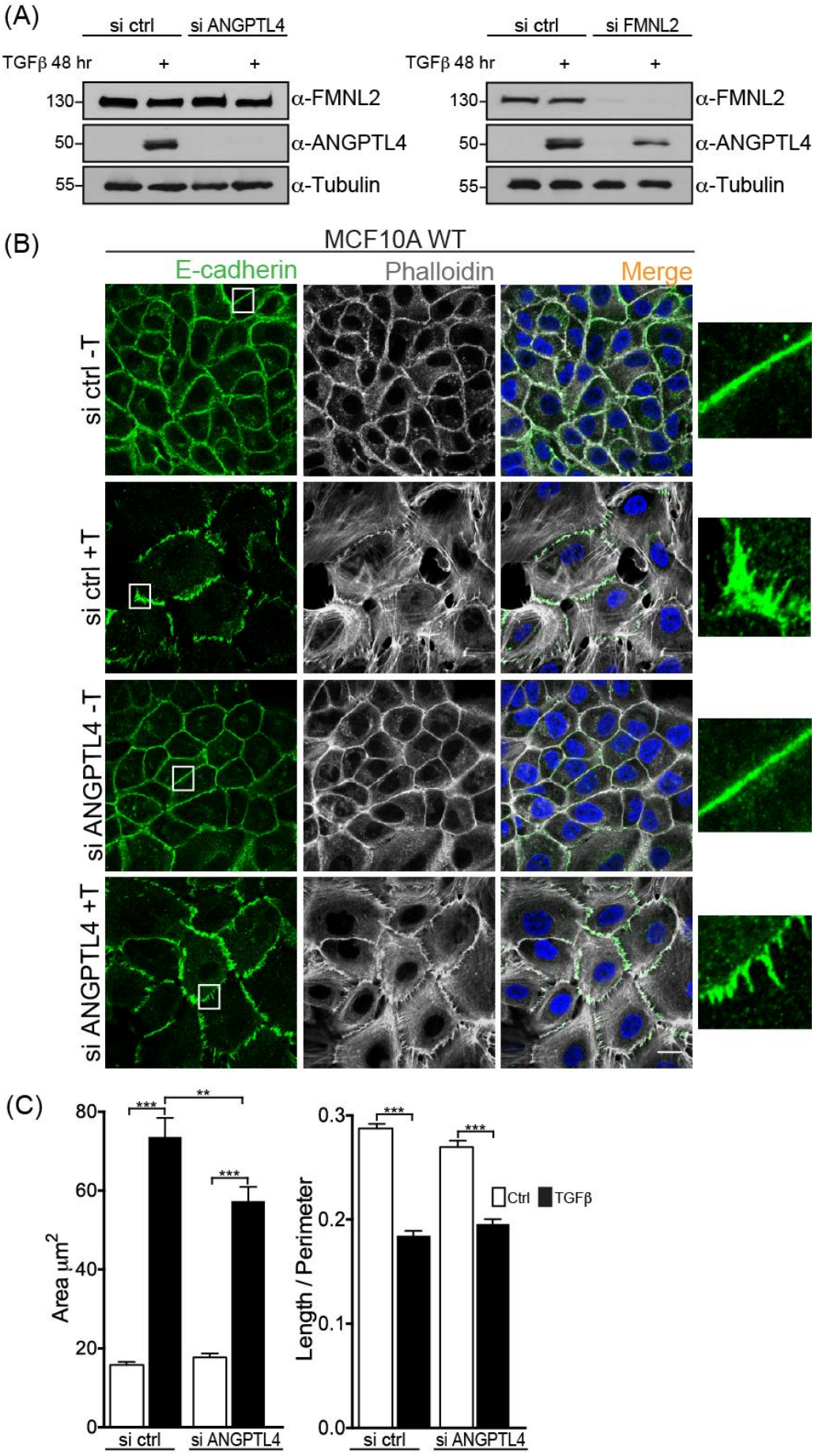

Figure 21. TGFβ-induced cell-cell contact changes in MCF10A WT cells.

(A) siRNA targeting ANGPTL4 or FMNL2 was transfected in MCF10A cells and the expression of both proteins was compared using immunoblotting. Scale bar, 20 μm **(B)** Cells were stimulated with TGFβ for 48 hr after siRNA transfection. They were further fixed and stained against E-cadherin and actin to visualize cell-cell contact integrity. **(C)** Quantification of the cell-cell contact area and length/perimeter. The white boxes serve as examples of the measured areas. Data is expressed as mean ± SEM, n ≤ 40. One-way ANOVA was performed to assess the significance.**p< 0.01, ***p< 0.001.

To monitor if the knockdown of ANGPTL4 had an effect on FMNL2 expression and vice versa, the proteins were silenced separately (Fig.21A). Reduction of ANGPTL4 had no effect on FMNL2 expression. However, we could observe less ANGPTL4 with FMNL2 knockdown. This is in line with our previous results which indicate a role of FMNL2 in ANGPTL4 secretion and hence in the availability of the protein inside the cells. ANGPTL4 was previously reported to disrupt cell-cell contacts and facilitate lung metastasis in mice (Huang et al., 2011). To more closely observe cell-cell contact changes influenced by ANGPTL4 in our model, we silenced the latter in MCF10A WT cells then stimulated for 48 hr with TGFβ (4 ng/mL). Cells were fixed and stained against E-cadherin and actin (Fig.21B). We chose to quantify cell-cell contact area and length/perimeter. Area showed an increase after TGFβ stimulation in the control and ANGPTL4 knockdown but to a lesser extent in the case of the knockdown. Length/Perimeter decreased accordingly in both cases (Fig.21C). An increase in cell-cell contact area indicates the disruption of the rigid and tight cell-cell contacts, leading to cell spreading and further migration. A decrease in length/perimeter signifies the disassembly of epithelial junctions and loss of the continuous cell boundaries. The FMNL2 KO cell line showed a modest increase in cell-cell contact area following TGFβ stimulation, around 60 μm^2, albeit lesser than the increase seen in the WT (80 μm^2). Upon ANGPTL4 silencing, we observed a pronounced decrease in cell-cell contact area reaching 30 μm^2 (Fig.22B) . Length/perimeter decreased in the knockout cell line after TGFβ stimulation, but this decrease was reversed upon ANGPTL4 silencing to rise back to 0.25. We conclude, that the combined loss of both FMNL2 and ANGPTL4 yields a much more prominent phenotype indicating a dual role of these two proteins in modulating cell-cell contact integrity during TGFβ-induced EMT.

4.6.2 Knockdown of ANGPTL4 in MCF10A FMNL2 KO cells

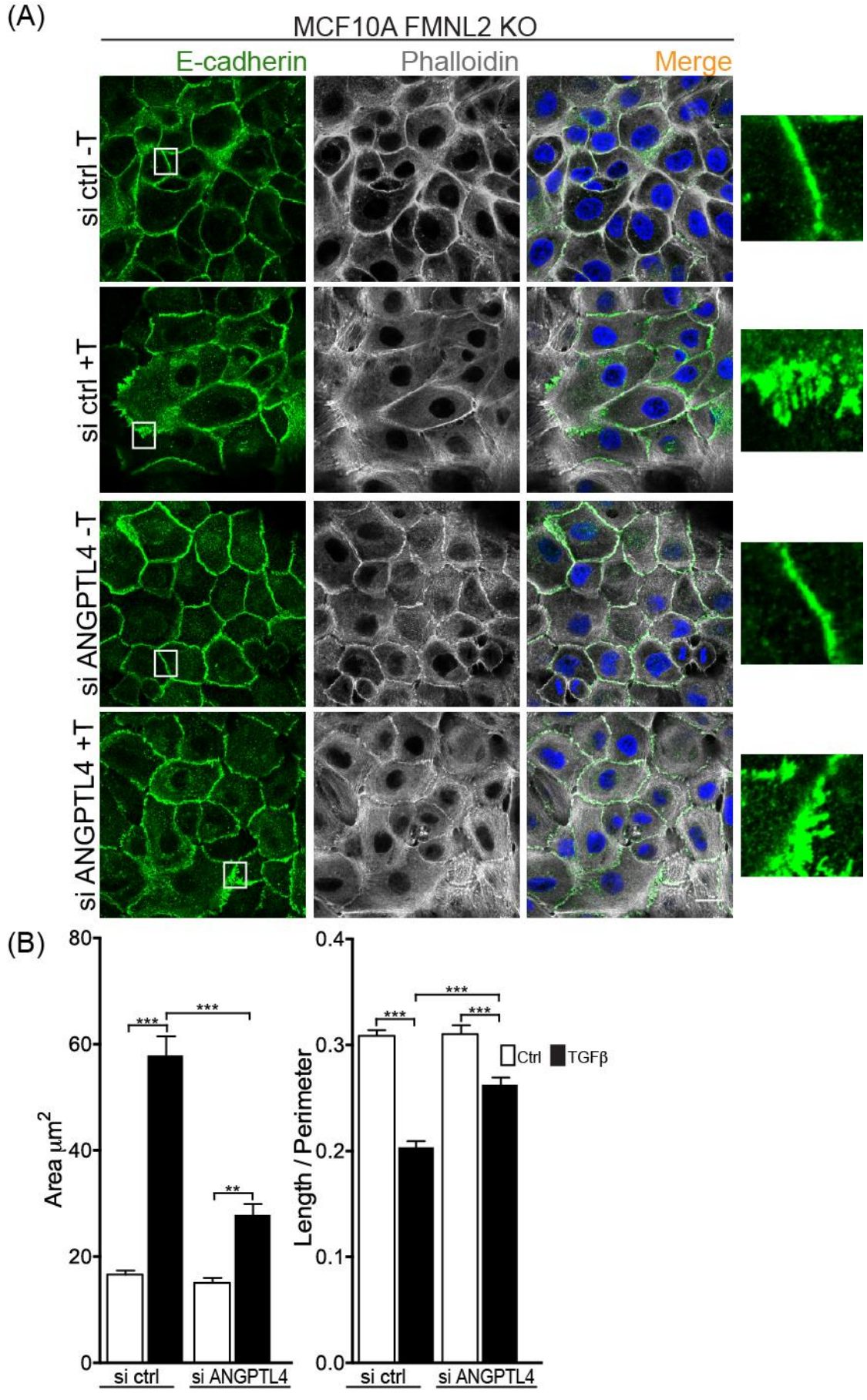

Figure 22. TGFβ-induced cell-cell contact changes in MCF10A FMNL2 KO cells.

(A) Cells were stimulated with TGFβ for 48 hr after siRNA transfection. They were further fixed and stained against E-cadherin and actin to visualize cell-cell contacts. Scale bar, 20 μm **(B)** Quantification of the cell-cell contact area and length/perimeter. The white boxes serve as examples of the measured areas. Zoom ins are displayed to the right. Data is expressed as mean ± SEM, n≤ 40. One-way ANOVA was performed to assess the significance.*p< 0.05,**p< 0.01, ***p< 0.001.

To monitor if the addition of ANGPTL4 could augment or rescue our phenotype, 1μg of recombinant ANGPTL4 protein was added to the cells along with TGFβ stimulation. We could observe a gain in the cell-cell contact area of the WT cells (Fig.23A,B) and a more pronounced difference in the length/perimeter parameter (ctrl vs. TGFβ +ANGPTL4). Hence, addition of exogenous ANGPTL4 aids in the disintegration of cell-cell contacts. Noticeably, the rescue effect in the FMNL2 KO cell line was evident. Upon addition of the ANGPTL4 protein, the cell-cell contact area proceeded to increase (90 μm_2) indicating disruption of the cell-cell contacts and spreading. Length/perimeter decreased accordingly from 0.3 to 0.15 upon TGFβ + ANGPTL4 protein addition (Fig.24 A,B). We infer that ANGPTL4 can rescue the FMNL2 knockout effect and drive EMT execution.

4.7 TGFβ-induced invasion requires both FMNL2 and ANGPTL4

Finally, to determine a dual role for ANGPTL4 and FMNL2 in tumorigenesis, we performed 3D inverted invasion assays. We transduced MCF10A FMNL2 cell lines with sh ctrl or sh ANGPTL4. The expression of the sh RNAs was induced with doxycycline and inverted invasion assays were performed. MCF10A WT cells showed a modest increase in invasion capacity after the 4-day stimulation with TGFβ reaching 8%. However, when FMNL2 was overexpressed, this increased to 37%. FMNL2 KO cell lines showed almost no invasion (1%), but this effect could be rescued when FMNL2 was re-introduced in the system (30%) but not by re-introducing the phospho-mutant (5%) (Fig. 25B). The invasion capacity of the WT and WT-FMNL2 cell lines was further reduced with the knockdown of ANGPTL4 (Fig.25C). However, invasion capacity of the FMNL2 KO cell line could not be rescued with the addition of the ANGPTL4 recombinant protein (Fig.25E). % invasion represents the number of cells which crossed the Matrigel barrier over the total number present on the bottom of the Matrigel. We conclude that TGFβ-induced invasion requires both FMNL2 and ANGPTL4.

4.6.3 Addition of ANGPTL4 in MCF10A WT cells

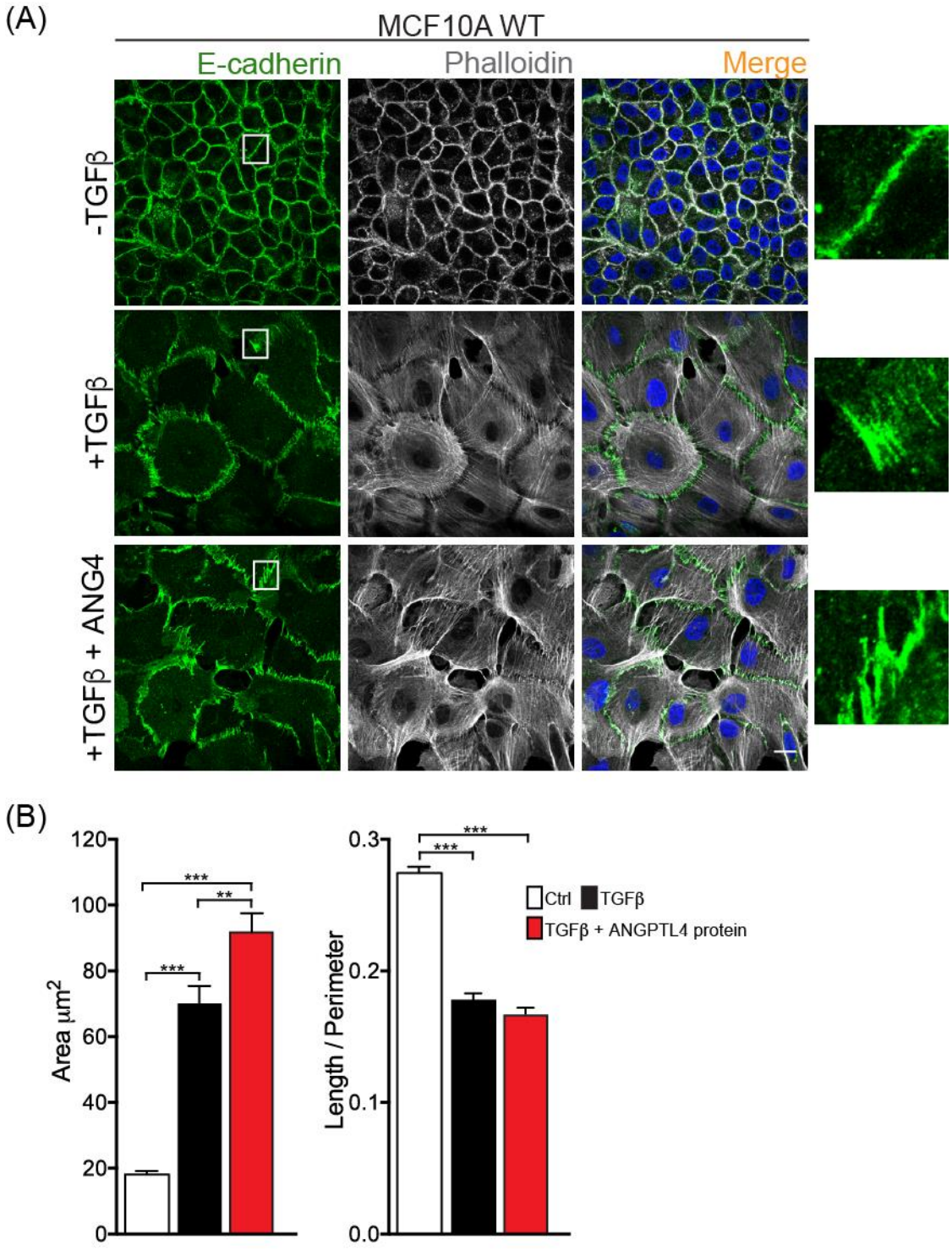

Figure 23. Influence of ANGPTL4 on TGFβ-induced cell-cell contact changes in MCF10A WT cells.

(A) WT cells were stimulated -/+TGFβ for 48 hr, along with the addition of 1 µg recombinant ANGPTL4. They were further fixed and stained against E-cadherin and actin to visualize cell-cell contacts. Scale bar, 20 µm **(B)** Quantification of the cell-cell contact area and length/perimeter.

The white boxes in **(A)** serve as examples of the measured areas. Data is expressed as mean ± SEM, n ≤ 40. One-way ANOVA was performed to assess the significance.**p< 0.01,***p< 0.001.

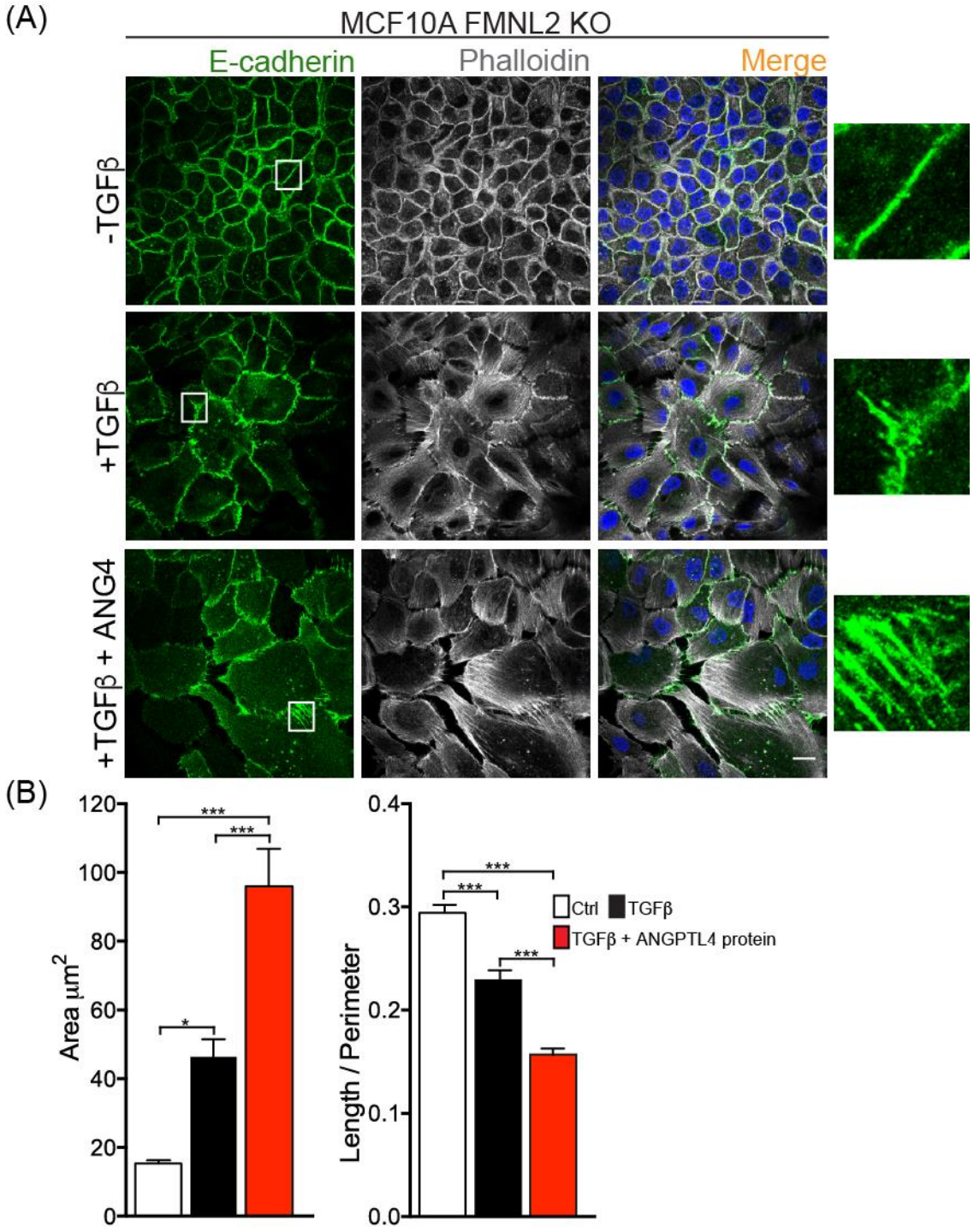

4.6.4 Addition of ANGPTL4 in MCF10A FMNL2 KO cells

Figure 24. Influence of ANGPTL4 on TGFβ-induced cell-cell contact changes in MCF10A KO cells.
(A) KO cells were stimulated -/+TGFβ for 48 hr, along with the addition of 1 µg recombinant ANGPTL4. They were further fixed and stained against E-cadherin and actin to visualize cell-cell contacts. Scale bar, 20 µm **(B)** Quantification of the cell-cell contact area and length/perimeter. The white boxes in **(A)** serve as examples of the measured areas. Data is expressed as mean ± SEM, n ≤ 40. One-way ANOVA was performed to assess the significance.*p< 0.5,***p< 0.001.

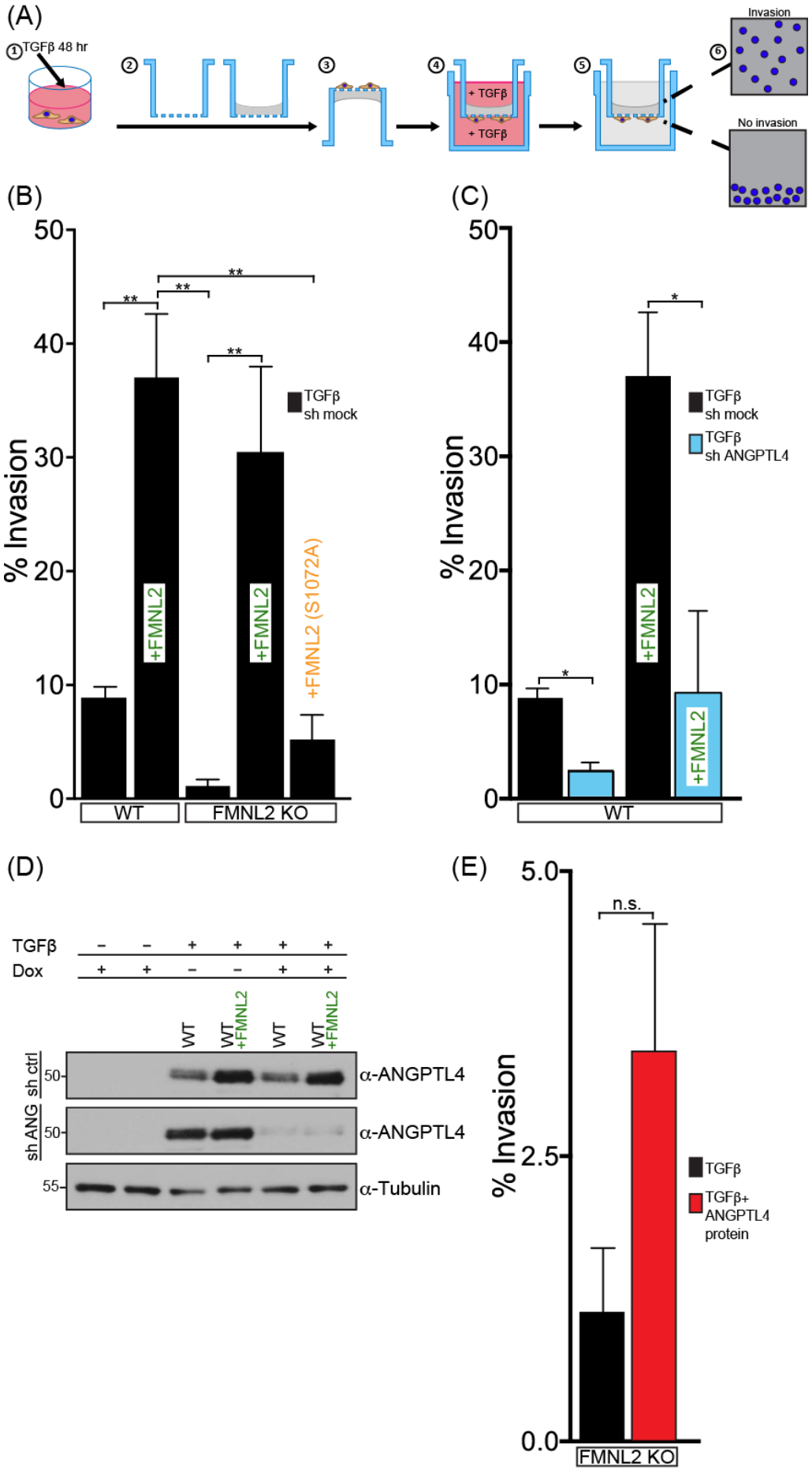
(A)
TGFβ 48 hr
+ TGFβ
+ TGFβ
Invasion
No invasion
(B)
% Invasion
TGFβ
sh mock
+FMNL2
+FMNL2
+FMNL2 (S1072A)
WT
FMNL2 KO
(C)
% Invasion
TGFβ
sh mock
TGFβ
sh ANGPTL4
+FMNL2
+FMNL2
WT
(D)
TGFβ
Dox
WT
WT +FMNL2
WT
WT +FMNL2
sh ctrl
sh ANG
α-ANGPTL4
α-ANGPTL4
α-Tubulin
(E)
% Invasion
n.s.
TGFβ
TGFβ+ ANGPTL4 protein
FMNL2 KO

Figure 25. TGFβ-dependent invasion requires FMNL2 in addition to ANGPTL4.
(A) Experimental setup of the 3D inverted invasion assay. Cells were treated with doxycycline (1 mg/mL) a day before the start of the experiment to induce the expression of shRNAs. The cells were stimulated with TGFβ for 48 hr (1) then plated upside down on a Matrigel-coated thincert (2,3). After incubation to allow cells to adhere, the thincert was placed in TGFβ containing medium (4) and the cells were allowed to invade for 48 hr through the Matrigel (5). They were then fixed and stained for DAPI to image invaded vs. non-invaded cells (6). **(B)** Different cell lines expressing sh ctrl were subjected to a 3D inverted invasion assay using Thincerts. % invasion is shown. Data is expressed as mean ± SEM, n=3. One-way ANOVA was performed to assess the significance.**p< 0.01,***p< 0.001. **(C)** sh ANGPTL4 was induced in the WT and most invasive cell line, WT (FMNL2-GFP) prior to the invasion assay. % Invasion is shown. Data is expressed as mean ± SEM, n=2. Student's t-test was performed to assess the significance.*p< 0.05. **(D)** Immunoblots confirming the efficiency of the shRNA in both WT and WT (+FMNL2) cell lines. **(E)** Recombinant ANGPTL4 protein (1 μg) was added to the Matrigel before beginning the assay. % Invasion is shown. Data is expressed as mean ± SEM, n=2. Student's t-test was performed to assess the significance. n.s. no significance.

5. Discussion

5.1 Role of the actin regulator, FMNL2, in the transcriptional program of the EMT process

Although the transcriptional program for EMT is well characterized and known to be coordinated primarily through activation of transcription factors such as Snail, ZEB, and Twist that repress expression of epithelial genes and activate expression of mesenchymal genes (Xu et al., 2009), less is known about how the morphological program of EMT is controlled and whether it also regulates transcriptional events. Cytoskeletal remodeling during EMT depends on changes in the expression of actin regulatory proteins, such as moesin (Haynes, Srivastava, Madson, Wittmann, & Barber, 2011), zyxin (Mori et al., 2009), and most importantly the formins (Jurmeister et al., 2012; Y. Y. Li, Jiang, Chen, Jiang, & Jiao, 2019; Yufa Li et al., 2010; Rana, Aloisio, Choi, & Barber, 2018). However, these regulators of the EMT morphological program are generally not necessary for transcriptional events with EMT. This correlated with our results, as we could observe that the knockout of FMNL2 had no effect on the induction of the transcriptional program. Smad2 was timely phosphorylated after stimulation with TGFβ and the epithelial markers were downregulated in the WT and FMNL2 KO MCF10A cell lines, with an upregulation of the mesenchymal markers.

5.2 PKC alpha upregulation in response to TGFβ and FMNL2 phosphorylation

Regulation of PKC activity by TGFβ has been previously reported. TGFβ stimulation increases PKCα mRNA, expression, and activity in fibroblasts (Gao et al., 2003a). PKCα further interacts with TGFβ receptor I and promotes its endocytosis in podocytes (Tossidou et al., 2009). Moreover, PKC phosphorylates Smad3 downstream of TGFβ signaling leading to down-regulation of growth inhibitory and apoptotic action of TGFβ (YAKYMOVYCH IHOR, PETER TEN DIJKE, CARL-HENRIK HELDIN, 2001). MCF10A cells are immortalized but non-transformed and non-tumorigenic, and we do not expect elevated PKC activity since that is found in human breast tumors (Kazanietz, 2015). This cell line expresses very low levels of PKCα and therefore offers a low background for experiments seeking to correlate overexpression of PKCα with its phenotypic consequences. Of the diacylglycerol (DAG)-sensitive isoforms expressed in these cells, PKCα is the only Ca^{2+}/DAG-dependent (conventional) isoform (Abeyweera, Chen, & Rotenberg, 2009). The upregulation we observe after TGFβ stimulation is in line with previous literature (Gao et al., 2003b; Zhou et al., 2009). Inhibition of FMNL2 phosphorylation upon BIM addition further confirms PKC involvement in our suggested

signaling pathway. This endorses our hypothesis where the phosphorylated form of FMNL2 is playing the more dominant and functional role during the initiation and execution of the EMT process following TGFβ stimulation.

5.3 ANGPTL4 as an FMNL2 interaction partner

Our experiments revealed ANGPTL4 as a cellular binding partner to FMNL2 under TGFβ-induced EMT conditions. ANGPTL4 binding appeared to be specific to the phosphorylated form of FMNL2, as the phospho-mutant (S1072A) showed no interaction in the immunoprecipitation assay. No other formins have been associated with endogenous ANGPTL4. Hence, the novelty of this interaction between an actin regulator and a matricellular glycoprotein is of great interest. Importantly, both FMNL2-NT and CT were able to directly interact with ANGPTL4. However, only the ANG NT showed an interaction with FMNL2. This could be due to the fact that ANGPTL4 has a predicted transmembrane domain in its NT which causes it to locate at cellular membranes and interact with FMNL2. The prediction software used determines the presence of alpha-helical membrane spanning regions. This has yet to be further verified experimentally, by X-ray or crystallography. We could not explain binding of ANGPTL4 to the C-terminal domain of FMNL2. However, removal of the signaling peptide was essential for the protein purification of ANGPTL4. We speculate that this could play a role in yielding unspecific interactions since the signaling peptide plays a role in proper targeting of the protein to the membrane and hence its possible interaction partners. To clarify this, we aim to perform Immunogold electron microscopy and use an antibody directed towards the N-terminus of ANGPTL4. We also consider isolating vesicles after TGFβ stimulation and probing for ANGPTL4-NT or ANGPTL4-CT to determine which form is more abundant, and hence is more probable to be interacting with FMNL2. Another option is obtaining a membrane-bound organelle fraction through membrane fractionation and probing for FMNL2 and/or ANGPTL4-NT. We can also attempt to mutate the putative transmembrane region of ANGPTL4 to abolish the ANGPTL4-FMNL2 interaction. Even though the cleavage site of ANGPTL4 is recognized, the distribution of the different isoforms and their tissue specificity is still not well defined. We assume that the cleavage is occurring either in the vesicles, or after ANGPTL4 secretion. Proprotein convertases such as Furin are enriched in the Golgi apparatus and are known to cleave ANGPTL4 (Lei et al., 2011). It would be of great interest to identify exactly which ANGPTL4 isoform is prevalent in our cell line and pinpoint its respective interaction with FMNL2.

We further show a critical role for FMNL2 in promoting the secretion of ANGPTL4 protein from secretory vesicles where FMNL2 KO diminishes the level of secreted ANGPTL4. Addition of different inhibitors targeted against actin (Latrunculin), formins (SMIFH2), or PKCs (BIM) showed no effect on the level of secretion. This could be due to the fact that we used low concentrations since the treatment was for a long period of 48 hr. Moreover, recent studies have implicated the role of formin mDia2 in stabilizing microtubules independently of their actin polymerization activity (Bartolini et al., 2008). Formins regulate cytoskeletal coordination where they mediate cross-talk between actin and microtubules. Hence, perhaps FMNL2 plays a role in regulating microtubules and the subsequent vesicle transport (Hehnly & Stamnes, 2007) or exocytosis (Müller et al., 2019). To test this, we could use the microtubule inhibitor nocodazole and monitor if secretion levels of ANGPTL4 are affected. Furthermore, ANGPTL4 was found to be accumulated in the Golgi and not in the extracellular matrix with the FMNL2 knockout or phospho-mutant background. This verifies that the absence of native FMNL2, and further phosphorylation, causes a secretion defect preventing ANGPTL4 release. The live imaging of FMNL2 and ANGPTL4 after TGFβ stimulation further confirmed this interaction and helped visualize the process of ANGPTL4 secretion.

Recently, loss of FMNL2/3 has been shown to result in altered Golgi architecture and a defect in anterograde vesicle trafficking (Kage, Steffen, et al., 2017). It is conceivable that FMNL-generated actin filaments might serve mechanical functions at the Golgi and during trafficking processes. Actin filaments are thought to contribute to the maintenance of the flattened shape of Golgi cisternae, and can facilitate membrane deformations driving processes such as vesicle formation, scission and fusion (Egea et al., 2013; Gurel, Hatch, & Higgs, 2014). However, we cannot exclude the crucial involvement of microtubules and their required interplay with actin to orchestrate vesicle trafficking. We conclude that FMNL2 and its further phosphorylation prompt the release of ANGPTL4 from secretory vesicles to the extracellular matrix.

5.4 Cell-cell contact changes accompanied by loss of FMNL2/ANGPTL4

In the human breast epithelial cell line MCF10A, FMNL2 specifically localizes to newly forming cell-cell contacts in 2D monolayers and 3D-cultured cells. Of note, in MCF10A cells depleted for FMNL2, contact formation but not lamellipodia protrusion was impaired, suggesting a cell-cell adhesion specific role for this formin. Consistent with this idea, FMNL2 physically associates with the junctional proteins α-catenin and E-cadherin, and the latter interaction is increased upon Rac1 activity (K Grikscheit et al., 2015). ANGPTL4 is a novel matricellular protein that was reported to interact with specific ECM

proteins and integrins to facilitate cell migration during wound healing. Matricellular proteins are extracellular matrix (ECM)-associated glycoproteins secreted by cancer cells and neighboring stromal cells into the environment. These proteins modulate cell-matrix interaction and are important factors in tumor progression (Wong & Rustgi, 2013). ANGPTL4 is highly expressed in metastatic cells, it enhances vascular permeability and promotes the metastasis of breast tumor cells to the lung and the metastasis of melanoma cells to the brain. Neutralizing antibody against cANGPTL4 resulted in tumor regression, reducing vascular disruption and thus, metastasis (Dao et al., 2019). Cells with FMNL2 KO and ANGPTL4 silencing failed to disrupt their cell-cell contacts and proceed through the EMT process. However, this phenotype could be rescued in the FMNL2 KO cell upon addition of recombinant ANGPTL4 and cell-cell contact disassembly presumed. These data point towards a cooperative function of FMNL2 and ANGPTL4 in modulating cell-cell contact integrity. Hence, in the absence of ANGPTL4 protein we can predict a decrease in the disruption of cell-cell contacts, less migration, and reduced metastasis. It would be of interest to observe the effect of Rac silencing in addition to ANGPTL4 silencing on cell-cell contacts' maintenance.

5.5 FMNL2 and ANGPTL4 are required for TGFβ-induced invasion

Finally, we show that the formin FMNL2 is critically involved in TGFβ-induced cancer cell invasion through 3D matrices. This experiment closely models amoeboid migration. In this experimental setup, migration requires that the cells identify pores in a membrane and squeeze through as single cells. Knockout of FMNL2 robustly diminishes the acquired invasive potential of MCF10A cells. This is in part consistent with recent findings showing that the knockdown of FMNL2 in A375 melanoma cell lines decreased their invasive potential (Wang et al., 2015). In addition, more ample evidence on the role of FMNL2 in cellular invasion further suggests and asserts that FMNL2 exerts migratory functions in cancer cells (Gardberg, Heuser, Koskivuo, Koivisto, & Carp En, n.d.; Kitzing et al., 2010; You Li et al., 2019; Péladeau, Heibein, Maltez, Copeland, & Copeland, 2016b; Zhong, Wang, Xu, & Kong, 2018; X.-L. Zhu et al., 2011; X. L. Zhu, Liang, & Ding, 2008b). Previously, other members of the DRF family have been demonstrated to play a role in invasive migration. mDia (Dia1) has been implicated in bleb-associated cancer cell invasion and knockdown of mDia1 efficiently inhibited the number of invading cells as well as the overall invaded distance (Kim et al., 2016). Two recent paper find mDia to be further involved in the EMT process as well (Rana et al., 2018; X.-L. Zhu et al., 2011). Thus, several formins appear to be relevant actin regulators for cancer cell motility and invasion either with overlapping or possibly with specific roles for different tumor cell

types and entities. These data strongly argue for a crucial and regulatory interaction between the formin FMNL2 and ANGPTL4 for invasive cell migration. We can speculate that the rounded and rapid single cancer cell motility is more efficient in seeding distant metastasis than the collective, mesenchymal mode of migration. The exact mechanism by which FMNL2 silencing reduces this kind of migration remains unexplained. It is possible that a subtle disruption of cell membrane structures affects their ability to sense the serum gradient, identify the pores or form focal complexes for adhesion. It is of importance here to clarify the role actin could essentially be playing in the invasive process. For that purpose, we will transduce FMNL2 KO cells expressing an actin-binding deficient mutant and test their invasion capacity.

ANGPTL4 has also been described to play a role in cancer cell invasion in breast and melanoma cancer models where cellular invasion is critically dependent on ANGPTL4 expression (Adhikary et al., 2013; Y. Sun, Long, & Zhou, 2014). Silencing of ANGPTL4 in our model further reduced the invasion capacity of the most invasive cell lines (WT and FMNL2-overexpressing). Here, we suggest that through the described interaction of ANGPTL4 with junctional components (Huang et al., 2011) and in line with our previous section **(5.4)**, that ANGPTL4 plays a role in disrupting cell contacts to promote invasion. This indicates the dual role FMNL2 and ANGPTL4 play in modulating TGFβ-induced cellular invasion.

5.6 Conclusion

In our study, we predicted a novel binding partner of the Formin-like 2 during TGFβ-induced epithelial mesenchymal transition. Initiating EMT in our non-transformed cell line led to PKC-alpha upregulation resulting in the activation of FMNL2 through a phospho-switch. We recognized Angiopoietin-like 4 to interact through its N-terminus with FMNL2 at cellular membranes. FMNL2 promotes ANGPTL4 secretion from intracellular vesicles and both act together in modulating cell-cell contact integrity and cellular invasiveness. An appealing future aspect is the possibility of employing formins such as FMNL2 as potential drug targets and matricellular glycoproteins, such as ANGPTL4, in the treatment of invasive diseases and particularly cancer.

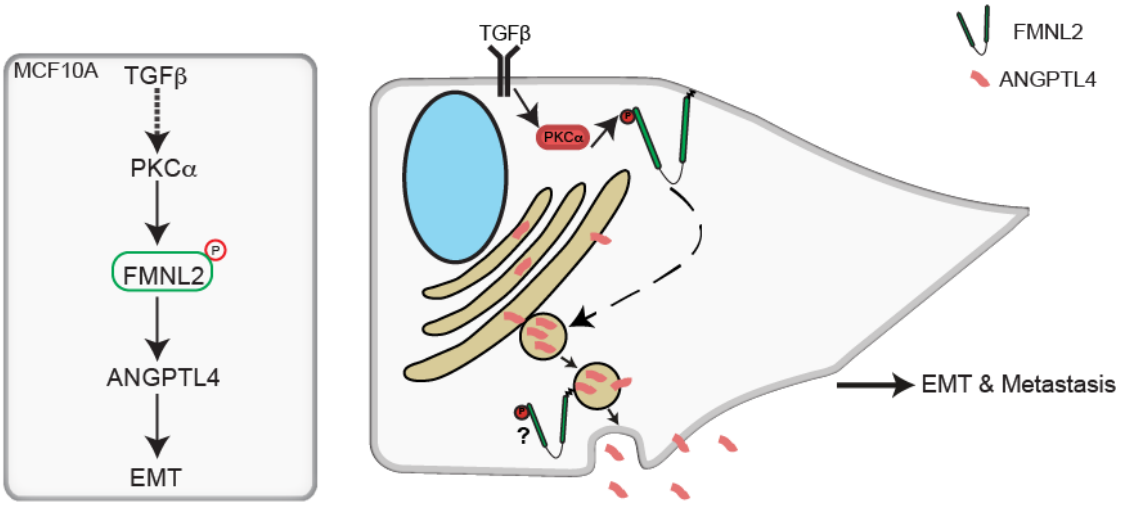

Figure 26. TGFβ targets Formin-like 2 for ANGPTL4 secretion in MCF10A WT cells during EMT.

Representative models summarizing the TGFβ-dependent phosphorylation of FMNL2 leading to its role in aiding secretion of ANGPTL4 to allow the cells to undergo EMT and further on metastasize.

6. Summary

Epithelial to Mesenchymal transition (EMT) is a highly dynamic process that plays a crucial role in tumor progression and metastasis. While remodelling of the actin cytoskeleton is a hallmark of EMT, the responsible actin regulating factors are less well understood. Formins are involved in numerous cellular mechanisms, ranging from cytokinesis to cell adhesion and motility. The Rho-GTPase effectors of the formin family compromise the largest group of actin nucleators and are emerging as relevant pharmacological targets. A critical role of Formin-like 2 (FMNL2) in the assembly of junctional actin at newly forming cell-cell contacts in a 3D matrix has been described. This activity originates downstream of Rac1 and is in line with a physical association of FMNL2 and components of the cadherin-catenin complex. FMNL2 was further recently implicated in β1-integrin trafficking as a direct PKC target required for cancer cell invasion.

Here we found that transforming growth factor-beta (TGFβ)-driven EMT leads to an upregulation of PKCα resulting in the phosphorylation and activation of FMNL2 in epithelial cells. Proteomic screening for TGFβ-mediated phospho-FMNL2 binding partners identified the tumor promotor ANGPTL4 as a specific binding partner. ANGPTL4 has important roles in cancer development and progression including promoting invasion and metastasis. We found that FMNL2 and ANGPTL4 directly interact under TGFβ-induced EMT. Our data show that FMNL2 is a critical regulator of ANGPTL4 secretion. Secretion of ANGPTL4 is diminished upon loss of FMNL2 and its phosphorylation. We further observed that ANGPTL4 is sequestered in the Golgi apparatus colocalizing with markers of the trans-Golgi network. Live imaging of vesicle secretion from the Golgi confirmed the transient co-localization of ANGPTL4 and FMNL2. Moreover, ANGPTL4 and FMNL2 modulate cell-cell contact integrity and ANGPTL4 silenced cells fail to disassemble their underlying cell-cell contacts to execute EMT. This effect was further enhanced upon FMNL2 knockout using FMNL2 CRISPR/Cas9 cell line. However, re-introduction of ANGPTL4 restored the mesenchymal phenotype and prompted the dissolution of cell-cell adhesions. Finally, we found that cellular invasion promoted by TGFβ depends on FMNL2 and is reduced upon ANGPTL4 silencing. Taken together, our data point towards a crucial role of FMNL2 for EMT via ANGPTL4 secretion.

Zusammenfassung

Epithelial-to-Mesenchymal Transition (EMT) beschreibt einen hochdynamischen Prozess, bei dem Epithelzellen Differenzierungsmerkmale mesenchymaler Zellen entwickeln. Dies spielt eine entscheidende Rolle bei der Tumorprogression und vereinfacht die Metastasierung von Krebszellen. Als Grundlage von EMT sind strukturelle Veränderungen im Aktinzytoskelett notwendig, jedoch sind die verantwortlichen, aktinregulierenden Faktoren nur unzureichend charakterisiert. Formine stellen hierbei eine Proteinfamilie dar, die an zahlreichen, zellulären Prozessen, wie der Zytokinese, der Adhäsion und der Motilität beteiligt ist. Als Rho-GTPase-Effektoren formen Formine die größte Gruppe bekannter Aktinnukleatoren und neuerdings auch pharmakologisch relevante Ziele. In diesem Kontext wurde eine entscheidende Rolle von Formin-like 2 (FMNL2) bei der Assemblierung von Aktinstrukturen an *de novo* gebildeten Zell-Zell-Kontakten in 3D-Zellkulturmodellen beschrieben. Diese Aktivität entsteht abwärts von Rac1 sowie durch eine direkte Interaktion von FMNL2 und Komponenten des Cadherin-Catenin-Komplexes. Darüber hinaus wurde eine Phosphorylierung von FMNL2 durch PKC als essentiell für den zellulären Stoffwechseln von β1-Integrinen und damit für die Invasion von Krebszellen herausgestellt.

In der vorliegenden Arbeit zeigen wir, dass die Transforming Growth Factor-beta (TGFβ)-induzierte EMT zu einer erhöhten Expression von PKCα führt, die in einer aktivierenden Phosphorylierung von FMNL2 in Epithelzellen resultiert. Das proteomische Screening von Phospho-FMNL2-Bindungspartner nach Behandlung mit TGFβ lieferte den Tumorpromotor ANGPTL4. ANGPTL4 spielt eine wichtige Rolle bei der Tumorentstehung und -progression, einschließlich der Förderung von Invasion und Metastasierung. Wir konnten nachweisen, dass FMNL2 und ANGPTL4 im Rahmen der TGFβ-induzierten EMT direkt interagieren. Unsere Daten weisen darauf hin, dass FMNL2 ein kritischer Regulator der ANGPTL4-Sekretion ist, da die Sekretion von ANGPTL4 durch den Verlust von FMNL2 und dessen Phosphorylierung verringert wird. Wir beobachteten weiterhin, dass ANGPTL4 im Golgi-Apparat mit Markern des trans-Golgi-Netzwerks kolokalisiert. Lebendzellmikroskopie der Vesikelsekretion aus dem Golgi-Apparat bestätigte die transiente Kolokalisation von ANGPTL4 und FMNL2. Des Weiteren modulieren ANGPTL4 und FMNL2 die Integrität von Zell-Zell-Kontakten, da ANGPTL4-defiziente Zellen Zell-Zell-Kontakte nicht zerlegen können, um EMT auszuführen. Dieser Defekt war bei Verlust von FMNL2 in einer FMNL2-CRISPR/Cas9-Zelllinie verstärkt. Eine ektopische Expression von ANGPTL4 stellte den

mesenchymalen Phänotyp wieder her und bewirkte die Auflösung von Zell-Zell-Kontakten. Schließlich fanden wir heraus, dass die TGFβ-induzierte Zellinvasion von FMNL2 abhängt und durch Verlust von ANGPTL4 reduziert wird. Zusammengenommen weisen unsere Daten auf eine essentielle Rolle von FMNL2 für die ANGPTL4-Sekretion und damit EMT hin.

7. References

Abeyweera, T. P., Chen, X., & Rotenberg, S. A. (2009). Phosphorylation of α6-tubulin by protein kinase Cα activates motility of human breast cells. *Journal of Biological Chemistry*, *284*(26), 17648–17656. https://doi.org/10.1074/jbc.M902005200

Adhikary, T., Brandt, D. T., Kaddatz, K., Stockert, J., Naruhn, S., Meissner, W., … Müller, R. (2013). Inverse PPARβ/δ agonists suppress oncogenic signaling to the ANGPTL4 gene and inhibit cancer cell invasion. *Oncogene*. https://doi.org/10.1038/onc.2012.549

Baarlink, C., Brandt, D., & Grosse, R. (2010). SnapShot: Formins. *Cell*. https://doi.org/10.1016/j.cell.2010.06.030

Bartolini, F., Moseley, J. B., Schmoranzer, J., Cassimeris, L., Goode, B. L., & Gundersen, G. G. (2008). The formin mDia2 stabilizes microtubules independently of its actin nucleation activity. *Journal of Cell Biology*, *181*(3), 523–536. https://doi.org/10.1083/jcb.200709029

Bindschadler, M., Osborn, E. A., Dewey, C. F., & McGrath, J. L. (2004). A Mechanistic Model of the Actin Cycle. *Biophysical Journal*. https://doi.org/10.1016/S0006-3495(04)74326-X

Blanchoin, L., Letort, G., Ennomani, H., Gressin, L., & Théry, M. (2015). Dynamic reorganization of the actin cytoskeleton. *F1000Research*. https://doi.org/10.12688/f1000research.6374.1

Block, J., Breitsprecher, D., K??hn, S., Winterhoff, M., Kage, F., Geffers, R., … Rottner, K. (2012). FMNL2 drives actin-based protrusion and migration downstream of Cdc42. *Current Biology*, *22*(11), 1005–1012. https://doi.org/10.1016/j.cub.2012.03.064

Block, J., Breitsprecher, D., Kühn, S., Winterhoff, M., Kage, F., Geffers, R., … Rottner, K. (2012). FMNL2 drives actin-based protrusion and migration downstream of Cdc42. *Current Biology*. https://doi.org/10.1016/j.cub.2012.03.064

Breitsprecher, D., Kiesewetter, A. K., Linkner, J., Vinzenz, M., Stradal, T. E. B., Small, J. V., … Faix, J. (2011). Molecular mechanism of Ena/VASP-mediated actin-filament elongation. *EMBO Journal*. https://doi.org/10.1038/emboj.2010.348

Bugyi, B., & Carlier, M.-F. (2010). Control of Actin Filament Treadmilling in Cell Motility. *Annual Review of Biophysics*. https://doi.org/10.1146/annurev-biophys-051309-103849

Campellone, K. G., & Welch, M. D. (2010). A nucleator arms race: cellular control of actin assembly. *Nature Reviews. Molecular Cell Biology*, *11*(4), 237–251. https://doi.org/10.1038/nrm2867

Castrillon, D. H., & Wasserman, S. A. (1994). diaphanous is required for cytokinesis in Drosophila and shares domains of similarity with the products of the limb deformity gene. *Development*.

Chaffer, C. L., San Juan, B. P., Lim, E., & Weinberg, R. A. (2016). EMT, cell plasticity and metastasis. *Cancer and Metastasis Reviews*. https://doi.org/10.1007/s10555-016-9648-7

Charras, G. T., Hu, C. K., Coughlin, M., & Mitchison, T. J. (2006). Reassembly of contractile actin cortex in cell blebs. *Journal of Cell Biology*. https://doi.org/10.1083/jcb.200602085

Chesarone, M. A., DuPage, A. G., & Goode, B. L. (2010). Unleashing formins to remodel the actin and microtubule cytoskeletons. *Nature Reviews. Molecular Cell Biology*, *11*(1), 62–74. https://doi.org/10.1038/nrm2816

Chesarone, M. A., & Goode, B. L. (2009). Actin nucleation and elongation factors: mechanisms and interplay. *Current Opinion in Cell Biology*. https://doi.org/10.1016/j.ceb.2008.12.001

Chhabra, E. S., & Higgs, H. N. (2006). INF2 is a WASP homology 2 motif-containing formin that severs actin filaments and accelerates both polymerization and depolymerization. *Journal of Biological Chemistry*. https://doi.org/10.1074/jbc.M604666200

Colón-Franco, J. M., Gomez, T. S., & Billadeau, D. D. (2011). Dynamic remodeling of the actin cytoskeleton by FMNL1γ is required for structural maintenance of the Golgi complex. *Journal of Cell Science*. https://doi.org/10.1242/jcs.083725

Cooper, G. M. (2000). Structure and {Organization} of {Actin} {Filaments}. *The Cell: A Molecular Approach. 2nd Edition*.

Courtemanche, N. (2018). Mechanisms of formin-mediated actin assembly and dynamics. *Biophysical Reviews*. https://doi.org/10.1007/s12551-018-0468-6

Dao, T., Gapihan, G., Leboeuf, C., Hamdan, D., Feugeas, J.-P., Tran, T., … Bousquet, G. (2019). Expression of Angiopoietin-like 4 Fibrinogen-Like Domain (cANGPTL4) increases risk of brain metastases in women with breast cancer. *The Breast*. https://doi.org/10.1016/s0960-9776(19)30129-8

Debnath, J., Muthuswamy, S. K., & Brugge, J. S. (2003). Morphogenesis and oncogenesis of MCF-10A mammary epithelial acini grown in three-dimensional basement membrane cultures. *Methods*. https://doi.org/10.1016/S1046-2023(03)00032-X

Derynck, R., & Zhang, Y. E. (2003). Smad-dependent and Smad-independent pathways in TGF-β family signalling. *Nature*. https://doi.org/10.1038/nature02006

DeWard, A. D., Eisenmann, K. M., Matheson, S. F., & Alberts, A. S. (2010). The role of formins in human disease. *Biochimica et Biophysica Acta - Molecular Cell Research*. https://doi.org/10.1016/j.bbamcr.2009.11.006

Dominguez, R. (2016). The WH2 Domain and Actin Nucleation: Necessary but Insufficient. *Trends in Biochemical Sciences*. https://doi.org/10.1016/j.tibs.2016.03.004

Dos Remedios, C. G., Chhabra, D., Kekic, M., Dedova, I. V., Tsubakihara, M., Berry, D. A., & Nosworthy, N. J. (2003). Actin binding proteins: Regulation of cytoskeletal microfilaments. *Physiological Reviews*. https://doi.org/10.1152/physrev.00026.2002

Egea, G., Serra-Peinado, C., Salcedo-Sicilia, L., & Gutiérrez-Martínez, E. (2013). Actin acting at the golgi. *Histochemistry and Cell Biology*. https://doi.org/10.1007/s00418-013-1115-8

Erfei, B., & Zigmond, S. H. (1999). Actin polymerization: Where the WASP stings. *Current Biology*. https://doi.org/10.1016/S0960-9822(99)80102-X

Faix, J., & Grosse, R. (2006). Staying in shape with formins. *Dev Cell*, *10*(6), 693–706. https://doi.org/S1534-5807(06)00209-7 [pii]10.1016/j.devcel.2006.05.001

Fletcher, D. A., & Mullins, R. D. (2010). Cell mechanics and the cytoskeleton. *Nature*. https://doi.org/10.1038/nature08908

Gao, P. J., Li, Y., Sun, A. J., Liu, J. J., Ji, K. D., Zhang, Y. Z., … Zhu, D. L. (2003a).

Differentiation of vascular myofibroblasts induced by transforming growth factor-β1 requires the involvement of protein kinase Cα. *Journal of Molecular and Cellular Cardiology*, *35*(9), 1105–1112. https://doi.org/10.1016/S0022-2828(03)00207-4

Gao, P. J., Li, Y., Sun, A. J., Liu, J. J., Ji, K. D., Zhang, Y. Z., … Zhu, D. L. (2003b). Differentiation of vascular myofibroblasts induced by transforming growth factor-β1 requires the involvement of protein kinase Cα. *Journal of Molecular and Cellular Cardiology*. https://doi.org/10.1016/S0022-2828(03)00207-4

Gardberg, M., Heuser, V. D., Koskivuo, I., Koivisto, M., & Carp En, O. (n.d.). FMNL2/FMNL3 formins are linked with oncogenic pathways and predict melanoma outcome. https://doi.org/10.1002/cjp2.34

Gardberg, M., Heuser, V. D., Koskivuo, I., Koivisto, M., & Carpén, O. (2016). FMNL2/FMNL3 formins are linked with oncogenic pathways and predict melanoma outcome. *The Journal of Pathology: Clinical Research*, *2*(1), 41–52. https://doi.org/10.1002/cjp2.34

Gauvin, T. J., Young, L. E., & Higgs, H. N. (2015). The formin FMNL3 assembles plasma membrane protrusions that participate in cell-cell adhesion. *Molecular Biology of the Cell*. https://doi.org/10.1091/mbc.E14-07-1247

Giannelli, G., Villa, E., & Lahn, M. (2014). Transforming growth factor-β as a therapeutic target in hepatocellular carcinoma. *Cancer Research*. https://doi.org/10.1158/0008-5472.CAN-14-0243

Goh, Y. Y., Pal, M., Chong, H. C., Zhu, P., Tan, M. J., Punugu, L., … Tan, N. S. (2010). Angiopoietin-like 4 interacts with integrins β1 and β5 to modulate keratinocyte migration. *American Journal of Pathology*. https://doi.org/10.2353/ajpath.2010.100129

Goley, E. D., Rodenbusch, S. E., Martin, A. C., & Welch, M. D. (2004). Critical conformational changes in the Arp2/3 complex are induced by nucleotide and nucleation promoting factor. *Molecular Cell*. https://doi.org/10.1016/j.molcel.2004.09.018

Goley, E. D., & Welch, M. D. (2006). The ARP2/3 complex: An actin nucleator comes of age. *Nature Reviews Molecular Cell Biology*. https://doi.org/10.1038/nrm2026

Goode, B. L., & Eck, M. J. (2007). Mechanism and function of formins in the control of actin assembly. *Annu Rev Biochem*, *76*, 593–627. https://doi.org/10.1146/annurev.biochem.75.103004.142647

Greenburg, G., & Hay, E. D. (1986). Cytodifferentiation and tissue phenotype change during transformation of embryonic lens epithelium to mesenchyme-like cells in vitro. *Developmental Biology*. https://doi.org/10.1016/0012-1606(86)90256-3

Grikscheit, K, Frank, T., Wang, Y., & Grosse, R. (2015). Junctional actin assembly is mediated by Formin-like 2 downstream of Rac1. *J Cell Biol*, *209*(3), 367–376. https://doi.org/jcb.201412015 [pii]10.1083/jcb.201412015

Grikscheit, Katharina, & Grosse, R. (2016). Formins at the Junction. *Trends in Biochemical Sciences*. https://doi.org/10.1016/j.tibs.2015.12.002

Grobe, H., Wü, A., Baarlink, C., Grosse, R., & Grikscheit, K. (2018). A Rac1-FMNL2 signaling module affects cell-cell contact formation independent of Cdc42 and membrane protrusions. https://doi.org/10.1371/journal.pone.0194716

Grodsky, N., Li, Y., Bouzida, D., Love, R., Jensen, J., Nodes, B., … Grant, S. (2006). Structure of the catalytic domain of human protein kinase C β II complexed with a

bisindolylmaleimide inhibitor. *Biochemistry*. https://doi.org/10.1021/bi061128h
Grootaert, C., Van De Wiele, T., Verstraete, W., Bracke, M., & Vanhoecke, B. (2012). Angiopoietin-like protein 4: Health effects, modulating agents and structure-function relationships. *Expert Review of Proteomics*. https://doi.org/10.1586/epr.12.12
Gurel, P. S., Hatch, A. L., & Higgs, H. N. (2014). Connecting the cytoskeleton to the endoplasmic reticulum and Golgi. *Current Biology*. https://doi.org/10.1016/j.cub.2014.05.033
Han, Y., Eppinger, E., Schuster, I. G., Weigand, L. U., Liang, X., Kremmer, E., … Krackhardt, A. M. (2009). Formin-like 1 (FMNL1) is regulated by N-terminal myristoylation and induces polarized membrane blebbing. *Journal of Biological Chemistry*. https://doi.org/10.1074/jbc.M109.060699
Hanahan, D., & Weinberg, R. A. (2011). Hallmarks of cancer: The next generation. *Cell*. https://doi.org/10.1016/j.cell.2011.02.013
Haynes, J., Srivastava, J., Madson, N., Wittmann, T., & Barber, D. L. (2011). Dynamic actin remodeling during epithelial-mesenchymal transition depends on increased moesin expression. *Molecular Biology of the Cell*. https://doi.org/10.1091/mbc.E11-02-0119
Hehnly, H., & Stamnes, M. (2007). Regulating cytoskeleton-based vesicle motility. *FEBS Letters*. https://doi.org/10.1016/j.febslet.2007.01.094
Hotulainen, P., & Lappalainen, P. (2006). Stress fibers are generated by two distinct actin assembly mechanisms in motile cells. *Journal of Cell Biology*. https://doi.org/10.1083/jcb.200511093
Huang, R. L., Teo, Z., Chong, H. C., Zhu, P., Tan, M. J., Tan, C. K., … Tan, N. S. (2011). ANGPTL4 modulates vascular junction integrity by integrin signaling and disruption of intercellular VE-cadherin and claudin-5 clusters. *Blood*, *118*(14), 3990–4002. https://doi.org/blood-2011-01-328716 [pii]10.1182/blood-2011-01-328716
Ireton, K. (2013). Molecular mechanisms of cell-cell spread of intracellular bacterial pathogens. *Open Biology*. https://doi.org/10.1098/rsob.130079
Iskratsch, T., Reijntjes, S., Dwyer, J., Toselli, P., Degano, I. R., Dominguez, I., & Ehler, E. (2013). Two distinct phosphorylation events govern the function of muscle FHOD3. *Cell Mol Life Sci*, *70*(5), 893–908. https://doi.org/10.1007/s00018-012-1154-7
Izraely, S., Ben-Menachem, S., Sagi-Assif, O., Meshel, T., Marzese, D. M., Ohe, S., … Witz, I. P. (2017). ANGPTL4 promotes the progression of cutaneous melanoma to brain metastasis. *Oncotarget*. https://doi.org/10.18632/oncotarget.19018
Jing, Y., Han, Z., Zhang, S., Liu, Y., & Wei, L. (2011). Epithelial-Mesenchymal Transition in tumor microenvironment. *Cell and Bioscience*. https://doi.org/10.1186/2045-3701-1-29
Jurmeister, S., Baumann, M., Balwierz, A., Keklikoglou, I., Ward, A., Uhlmann, S., … Sahin, O. (2012). MicroRNA-200c represses migration and invasion of breast cancer cells by targeting actin-regulatory proteins FHOD1 and PPM1F. *Mol Cell Biol*, *32*(3), 633–651. https://doi.org/MCB.06212-11 [pii]10.1128/MCB.06212-11
Kage, F., Steffen, A., Ellinger, A., Ranftler, C., Gehre, C., Brakebusch, C., … Rottner, K. (2017). FMNL2 and -3 regulate Golgi architecture and anterograde transport downstream of Cdc42. *Scientific Reports*. https://doi.org/10.1038/s41598-017-

09952-1
Kage, F., Winterhoff, M., Dimchev, V., Mueller, J., Thalheim, T., Freise, A., … Rottner, K. (2017). FMNL formins boost lamellipodial force generation. *Nature Communications*. https://doi.org/10.1038/ncomms14832
Kazanietz, M. G. (2015). Protein kinase C and cancer : what we know and what we do not, *33*(45), 5225–5237. https://doi.org/10.1038/onc.2013.524.Protein
Kim, D., Jung, J., You, E., Ko, P., Oh, S., & Rhee, S. (2016). mDia1 regulates breast cancer invasion by controlling membrane type 1-matrix metalloproteinase localization. *Oncotarget*. https://doi.org/10.18632/oncotarget.7429
Kitzing, T. M., Wang, Y., Pertz, O., Copeland, J. W., & Grosse, R. (2010). Formin-like 2 drives amoeboid invasive cell motility downstream of RhoC. *Oncogene*. https://doi.org/10.1038/onc.2009.515
Kovar, D. R., & Pollard, T. D. (2004). Progressing actin: Formin as a processive elongation machine. *Nature Cell Biology*. https://doi.org/10.1038/ncb1204-1158
Kühn, S., & Geyer, M. (2014). Formins as effector proteins of Rho GTPases. *Small GTPases*, *5*(June), 1–16. https://doi.org/10.4161/sgtp.29513
Lammers, M., Rose, R., Scrima, A., & Wittinghofer, A. (2005). The regulation of mDia1 by autoinhibition and its release by Rho*GTP. *EMBO J*, *24*(23), 4176–4187. https://doi.org/7600879 [pii]10.1038/sj.emboj.7600879
Lamouille, S., Xu, J., & Derynck, R. (2014). Molecular mechanisms of epithelial-mesenchymal transition. *Nature Reviews Molecular Cell Biology*. https://doi.org/10.1038/nrm3758
Le Clainche, C., & Carlier, M. F. (2008). Regulation of actin assembly associated with protrusion and adhesion in cell migration. *Physiological Reviews*. https://doi.org/10.1152/physrev.00021.2007
Le Jan, S., Amy, C., Cazes, A., Monnot, C., Lamandé, N., Favier, J., … Germain, S. (2003). Angiopoietin-like 4 is a proangiogenic factor produced during ischemia and in conventional renal cell carcinoma. *American Journal of Pathology*. https://doi.org/10.1016/S0002-9440(10)64285-X
Lee, S. H., & Dominguez, R. (2010). Regulation of actin cytoskeleton dynamics in cells. *Molecules and Cells*. https://doi.org/10.1007/s10059-010-0053-8
Lei, X., Shi, F., Basu, D., Huq, A., Routhier, S., Day, R., & Jin, W. (2011). Proteolytic processing of angiopoietin-like protein 4 by proprotein convertases modulates its inhibitory effects on lipoprotein lipase activity. *Journal of Biological Chemistry*. https://doi.org/10.1074/jbc.M110.217638
Li, B., Qian, M., Cao, H., Jia, Q., Wu, Z., Yang, X., … Xiao, J. (2017). TGF-β2-induced ANGPTL4 expression promotes tumor progression and osteoclast differentiation in giant cell tumor of bone. *Oncotarget*. https://doi.org/10.18632/oncotarget.18629
Li, H., Xu, F., Li, S., Zhong, A., Meng, X., & Lai, M. (2016). The tumor microenvironment: An irreplaceable element of tumor budding and epithelial-mesenchymal transition-mediated cancer metastasis. *Cell Adhesion and Migration*. https://doi.org/10.1080/19336918.2015.1129481
Li, Y. Y., Jiang, G. T., Chen, L. J., Jiang, Y. H., & Jiao, J. D. (2019). Formin mDia1 contributes to migration and epithelial-mesenchymal transition of tubular epithelial cells exposed to TGF-β1. *Journal of Cellular Biochemistry*. https://doi.org/10.1002/jcb.29508

Li, You, Zhang, Q., Liu, F., Zhang, Z., Zou, Y., Yang, B., … Huang, O. (2019). Inhibition of formin like 2 promotes the transition of ectopic endometrial stromal cells to epithelial cells in adenomyosis through a MET-like process. *Gene*, *710*, 186–192. https://doi.org/10.1016/J.GENE.2019.06.003

Li, Yufa, Zhu, X., Zeng, Y., Wang, J., Zhang, X., Ding, Y., & Liang, L. (2010). FMNL2 enhances invasion of colorectal carcinoma by inducing epithelial-mesenchymal transition. *Molecular Cancer Research : MCR*, *8*(12), 1579–1590. https://doi.org/10.1158/1541-7786.MCR-10-0081

Liang, L., Li, X., Zhang, X., Lv, Z., He, G., Zhao, W., … Ding, Y. (2013). MicroRNA-137, an HMGA1 target, suppresses colorectal cancer cell invasion and metastasis in mice by directly targeting FMNL2. *Gastroenterology*. https://doi.org/10.1053/j.gastro.2012.11.033

Macara, I. G., Guyer, R., Richardson, G., Huo, Y., & Ahmed, S. M. (2014). Epithelial homeostasis. *Current Biology*. https://doi.org/10.1016/j.cub.2014.06.068

Machesky, L. M., Atkinson, S. J., Ampe, C., Vandekerckhove, J., & Pollard, T. D. (1994). Purification of a cortical complex containing two unconventional actins from Acanthamoeba by affinity chromatography on profilin-agarose. *Journal of Cell Biology*. https://doi.org/10.1083/jcb.127.1.107

Miyagi, Y., Yamashita, T., Fukaya, M., Sonoda, T., Okuno, T., Yamada, K., … Yokohama. (2002). Delphilin: A novel PDZ and formin homology domain-containing protein that synaptically colocalizes and interacts with glutamate receptor δ2 subunit. *Journal of Neuroscience*. https://doi.org/10.1523/jneurosci.22-03-00803.2002

Mizuno, H., Tanaka, K., Yamashiro, S., Narita, A., & Watanabe, N. (2018). Helical rotation of the diaphanous-related formin mDia1 generates actin filaments resistant to cofilin. *Proceedings of the National Academy of Sciences of the United States of America*. https://doi.org/10.1073/pnas.1803415115

Mori, M., Nakagami, H., Koibuchi, N., Miura, K., Takami, Y., Koriyama, H., … Kaneda, Y. (2009). Zyxin mediates actin fiber reorganization in epithelial-mesenchymal transition and contributes to endocardial morphogenesis. *Molecular Biology of the Cell*. https://doi.org/10.1091/mbc.E09-01-0046

Moriya, K., Yamamoto, T., Takamitsu, E., Matsunaga, Y., Kimoto, M., Fukushige, D., … Utsumi, T. (2012). Protein N-myristoylation is required for cellular morphological changes induced by two formin family proteins, FMNL2 and FMNL3. *Bioscience, Biotechnology, and Biochemistry*, *76*(6), 1201–1209. https://doi.org/10.1271/bbb.120069

Müller, M. T., Schempp, R., Lutz, A., Felder, T., Felder, E., & Miklavc, P. (2019). Interaction of microtubules and actin during the post-fusion phase of exocytosis. *Scientific Reports*. https://doi.org/10.1038/s41598-019-47741-0

Narumiya, S., Tanji, M., & Ishizaki, T. (2009). Rho signaling, ROCK and mDia1, in transformation, metastasis and invasion. *Cancer and Metastasis Reviews*. https://doi.org/10.1007/s10555-008-9170-7

Nurnberg, A., Kitzing, T., & Grosse, R. (2011). Nucleating actin for invasion. *Nat Rev Cancer*, *11*(3), 177–187. https://doi.org/nrc3003 [pii]10.1038/nrc3003

Olson, M. F., & Sahai, E. (2009). The actin cytoskeleton in cancer cell motility. *Clinical & Experimental Metastasis*, *26*(4), 273–287. https://doi.org/10.1007/s10585-008-9174-2

Otterbein, L. R., Graceffa, P., & Dominguez, R. (2001). The crystal structure of

uncomplexed actin in the ADR state. *Science*. https://doi.org/10.1126/science.1059700

Padua, D, Zhang, X. H., Wang, Q., Nadal, C., Gerald, W. L., Gomis, R. R., & Massague, J. (2008). TGFbeta primes breast tumors for lung metastasis seeding through angiopoietin-like 4. *Cell*, *133*(1), 66–77. https://doi.org/S0092-8674(08)00211-0 [pii]10.1016/j.cell.2008.01.046

Padua, David, Zhang, X. H. F., Wang, Q., Nadal, C., Gerald, W. L., Gomis, R. R., & Massagué, J. (2008). TGFβ Primes Breast Tumors for Lung Metastasis Seeding through Angiopoietin-like 4. *Cell*. https://doi.org/10.1016/j.cell.2008.01.046

Parsons, J. T., Horwitz, A. R., & Schwartz, M. A. (2010). Cell adhesion: Integrating cytoskeletal dynamics and cellular tension. *Nature Reviews Molecular Cell Biology*. https://doi.org/10.1038/nrm2957

Paul, A. S., & Pollard, T. D. (2009). Review of the mechanism of processive actin filament elongation by formins. *Cell Motility and the Cytoskeleton*. https://doi.org/10.1002/cm.20379

Péladeau, C., Heibein, A., Maltez, M. T., Copeland, S. J., & Copeland, J. W. (2016a). A specific FMNL2 isoform is up-regulated in invasive cells. https://doi.org/10.1186/s12860-016-0110-z

Péladeau, C., Heibein, A., Maltez, M. T., Copeland, S. J., & Copeland, J. W. (2016b). A specific FMNL2 isoform is up-regulated in invasive cells. *BMC Cell Biology*, *17*(1). https://doi.org/10.1186/s12860-016-0110-z

Pollard, T. D. (2016). Actin and actin-binding proteins. *Cold Spring Harbor Perspectives in Biology*. https://doi.org/10.1101/cshperspect.a018226

Pollard, T. D., & Cooper, J. A. (2009). Actin, a central player in cell shape and movement. *Science*. https://doi.org/10.1126/science.1175862

Prehoda, K. E., Scott, J. A., Mullins, R. D., & Lim, W. A. (2000). Integration of multiple signals through cooperative regulation of the N-WASP-Arp2/3 complex. *Science*. https://doi.org/10.1126/science.290.5492.801

Rana, M. K., Aloisio, F. M., Choi, C., & Barber, D. L. (2018). Formin-dependent TGF-β signaling for epithelial to mesenchymal transition. *Molecular Biology of the Cell*, *29*(12), 1465–1475. https://doi.org/10.1091/mbc.E17-05-0325

Reymond, N., D'Água, B. B., & Ridley, A. J. (2013). Crossing the endothelial barrier during metastasis. *Nature Reviews Cancer*. https://doi.org/10.1038/nrc3628

Rouiller, I., Xu, X. P., Amann, K. J., Egile, C., Nickell, S., Nicastro, D., … Hanein, D. (2008). The structural basis of actin filament branching by the Arp2/3 complex. *Journal of Cell Biology*. https://doi.org/10.1083/jcb.200709092

Sept, D., & McCammon, J. A. (2001). Thermodynamics and kinetics of actin filament nucleation. *Biophysical Journal*. https://doi.org/10.1016/S0006-3495(01)75731-1

Severson, A. F., Baillie, D. L., & Bowerman, B. (2002). A Formin Homology protein and a profilin are required for cytokinesis and Arp2/3-independent assembly of cortical microfilaments in C. elegans. *Current Biology*. https://doi.org/10.1016/S0960-9822(02)01355-6

Shimada, A., Vetter, I. R., Narumiya, S., Ku, D., Geeves, M. A., & Wittinghofer, A. (2004). The Core FH2 Domain of Diaphanous-Related Formins Is an Elongated Actin Binding Protein that Inhibits Polymerization. *Molecular Cell*.

Steinberg, S. F. (2008). Structural basis of protein kinase C isoform function. *Physiological Reviews*. https://doi.org/10.1152/physrev.00034.2007

Sun, N., Taguchi, A., & Hanash, S. (2016). Switching Roles of TGF-β in Cancer Development: Implications for Therapeutic Target and Biomarker Studies. *Journal of Clinical Medicine*. https://doi.org/10.3390/jcm5120109

Sun, Y., Long, J., & Zhou, Y. (2014). Angiopoietin-like 4 promotes melanoma cell invasion and survival through aldolase A. *Oncology Letters*. https://doi.org/10.3892/ol.2014.2071

Takeya, R., Taniguchi, K., Narumiya, S., & Sumimoto, H. (2008). The mammalian formin FHOD1 is activated through phosphorylation by ROCK and mediates thrombin-induced stress fibre formation in endothelial cells. *The EMBO Journal*, *27*(4), 618–628. https://doi.org/10.1038/emboj.2008.7

Tan, M. J., Teo, Z., Sng, M. K., Zhu, P., & Tan, N. S. (2012). Emerging roles of angiopoietin-like 4 in human cancer. *Molecular Cancer Research*. https://doi.org/10.1158/1541-7786.MCR-11-0519

Tossidou, I., Starker, G., Krüger, J., Meier, M., Leitges, M., Haller, H., & Schiffer, M. (2009). PKC-alpha modulates TGF-β signaling and impairs podocyte survival. *Cellular Physiology and Biochemistry*. https://doi.org/10.1159/000257518

Tsai, J. H., & Yang, J. (2013). Epithelial-mesenchymal plasticity in carcinoma metastasis. *Genes and Development*. https://doi.org/10.1101/gad.225334.113

Tseng, Y., Kole, T. P., Lee, J. S. H., Fedorov, E., Almo, S. C., Schafer, B. W., & Wirtz, D. (2005). How actin crosslinking and bundling proteins cooperate to generate an enhanced cell mechanical response. *Biochemical and Biophysical Research Communications*. https://doi.org/10.1016/j.bbrc.2005.05.205

Vaillant, D. C., Copeland, S. J., Davis, C., Thurston, S. F., Abdennur, N., & Copeland, J. W. (2008). Interaction of the N- and C-terminal autoregulatory domains of FRL2 does not inhibit FRL2 activity. *Journal of Biological Chemistry*. https://doi.org/10.1074/jbc.M803156200

Volkmann, N., Amann, K. J., Stoilova-McPhie, S., Egile, C., Winter, D. C., Hazelwood, L., … Hanein, D. (2001). Structure of arp2/3 complex in its activated state and in actin filament branch junctions. *Science*. https://doi.org/10.1126/science.1063025

Wang, Y., Arjonen, A., Pouwels, J., Ta, H., Pausch, P., Bange, G., … Grosse, R. (2015). Formin-like 2 Promotes beta1-Integrin Trafficking and Invasive Motility Downstream of PKCalpha. *Dev Cell*, *34*(4), 475–483. https://doi.org/S1534-5807(15)00422-0 [pii]10.1016/j.devcel.2015.06.015

Welm, A. L. (2008). TGFβ Primes Breast Tumor Cells for Metastasis. *Cell*. https://doi.org/10.1016/j.cell.2008.03.012

Wong, G. S., & Rustgi, A. K. (2013). Matricellular proteins: Priming the tumour microenvironment for cancer development and metastasis. *British Journal of Cancer*. https://doi.org/10.1038/bjc.2012.592

Wu, Y., & Zhou, B. P. (2009). Inflammation: A driving force speeds cancer metastasis. *Cell Cycle*. https://doi.org/10.4161/cc.8.20.9699

Xu, J., Lamouille, S., & Derynck, R. (2009). TGF-B-induced epithelial to mesenchymal transition. *Cell Research*. https://doi.org/10.1038/cr.2009.5

YAKYMOVYCH IHOR, PETER TEN DIJKE, CARL-HENRIK HELDIN, and S. S. (2001). Regulation of Smad signaling by protein kinase C. *FASEB*.

Yan, Y., Wang, Z., & Qin, B. (2019). A novel long noncoding RNA, LINC00483 promotes proliferation and metastasis via modulating of FMNL2 in CRC. *Biochemical and Biophysical Research Communications*.

https://doi.org/10.1016/j.bbrc.2018.12.090
Young, K. G., & Copeland, J. W. (2010). Formins in cell signaling. *Biochimica et Biophysica Acta - Molecular Cell Research*. https://doi.org/10.1016/j.bbamcr.2008.09.017
Zhang, J., Tian, X.-J. X.-J., Zhang, H., Teng, Y., Li, R., Bai, F., … Xing, J. (2014). TGF- -induced epithelial-to-mesenchymal transition proceeds through stepwise activation of multiple feedback loops. *Science Signaling*, *7*(345), ra91–ra91. https://doi.org/10.1126/scisignal.2005304
Zhong, B., Wang, K., Xu, H., & Kong, F. (2018). Silencing Formin-like 2 inhibits growth and metastasis of gastric cancer cells through suppressing internalization of integrins. *Cancer Cell Int*, *18*, 79. https://doi.org/10.1186/s12935-018-0576-1
Zhou, H. Y., Chen, W. D., Zhu, D. L., Wu, L. Y., Zhang, J., Han, W. Q., … Gao, P. J. (2009). The PDE1A-PKCα signaling pathway is involved in the upregulation of α-smooth muscle actin by TGF-β1 in adventitial fibroblasts. *Journal of Vascular Research*. https://doi.org/10.1159/000231716
Zhu, P, Goh, Y. Y., Chin, H. F., Kersten, S., & Tan, N. S. (2012). Angiopoietin-like 4: a decade of research. *Biosci Rep*, *32*(3), 211–219. https://doi.org/BSR20110102 [pii]10.1042/BSR20110102
Zhu, Pengcheng, Tan, M. J., Huang, R. L., Tan, C. K., Chong, H. C., Pal, M., … Tan, N. S. (2011). Angiopoietin-like 4 Protein Elevates the Prosurvival Intracellular O2-:H2O2 Ratio and Confers Anoikis Resistance to Tumors. *Cancer Cell*. https://doi.org/10.1016/j.ccr.2011.01.018
Zhu, X.-L., Zeng, Y.-F., Guan, J., Li, Y.-F., Deng, Y.-J., Bian, X.-W., … Liang, L. (2011). FMNL2 is a positive regulator of cell motility and metastasis in colorectal carcinoma. *The Journal of Pathology*, *224*(3), 377–388. https://doi.org/10.1002/path.2871
Zhu, X. L., Liang, L., & Ding, Y. Q. (2008a). Overexpression of FMNL2 is closely related to metastasis of colorectal cancer. *International Journal of Colorectal Disease*. https://doi.org/10.1007/s00384-008-0520-2
Zhu, X. L., Liang, L., & Ding, Y. Q. (2008b). Overexpression of FMNL2 is closely related to metastasis of colorectal cancer. *International Journal of Colorectal Disease*, *23*(11), 1041–1047. https://doi.org/10.1007/s00384-008-0520-2
Zimmermann, J., & Falcke, M. (2014). Formation of transient lamellipodia. *PLoS ONE*. https://doi.org/10.1371/journal.pone.0087638